**DELPHI Collaboration**
Track and Vertex Reconstruction

DELPHI 88-46 / PROG-112
25 June 1988

# VERTEX EVALUATION IN THE DELPHI EXPERIMENT

(Strategies and first results from Monte-Carlo data)

**Winfried A. Mitaroff**
Institut für Hochenergiephysik der ÖAW
Vienna, Austria

Presented at the XVI$^{th}$ Int. Meeting on Fundamental Physics, Peñíscola (Spain), 25-29 April 1988.

# VERTEX EVALUATION IN THE DELPHI EXPERIMENT

(Strategies and first results from Monte-Carlo data)

**Winfried A. Mitaroff**
Institut für Hochenergiephysik der ÖAW
Vienna, Austria

## Abstract

At the new $e^+e^-$ storage ring (LEP) at CERN, reactions with complex decays of heavy particles will be of particular interest. The more stable ones (like B and D mesons, $\tau$ lepton) have lifetimes greater than $10^{-13}$ sec; evaluation of their decay vertices thus requires a spatial resolution of ca. 10 $\mu$m.

For this aim, the DELPHI spectrometer contains a vertex detector (silicon micro-strips). Also needed is optimal utilization of all measurement information and correct treatment of multiple scattering for the geometrical reconstruction of tracks and vertices. Since the straightforward method of least-squares fitting leads to prohibitive computing times, more sophisticated algorithms (which are equivalent to the Kalman filter) must be used.

First results from Monte-Carlo studies on the precision of track and vertex fitting confirm the usefulness of these methods.

Presented at the XVI$^{th}$ Int. Meeting on Fundamental Physics, Peñíscola (Spain), 25-29 April 1988.

**Table of Contents**

## Introduction

Heavy flavour physics will play an important role in the research program at CERN's $e^+e^-$ storage ring LEP [1]. The DELPHI experiment will be outstanding for its capability of hadron identification by means of RICH detectors covering the full solid angle [2]. This advantage needs to be complemented by being able to reconstruct in space the decay vertices of charm and bottom mesons.

The decay properties of some particles of interest are summarized below [3]:

| Particle | $\bar{\tau}$ / sec | $c*\bar{\tau}$ | decay topology | comments |
|---|---|---|---|---|
| $K^0_L$ | $5.2*10^{-8}$ | 1554 cm | V2 | excluded |
| $K^\pm$ | $1.2*10^{-8}$ | 371 cm | C1, 3 | global PR |
| $\Lambda^0$ | $2.6*10^{-10}$ | 7.9 cm | V2 | important |
| $K^0_S$ | $0.9*10^{-10}$ | 2.7 cm | V2 | -- " -- |
| $B^0$, $B^\pm$ | $1.4*10^{-12}$ | 420 µm | V4, 6; C3, 5, 7 | desirable |
| $D^\pm$ | $9.2*10^{-13}$ | 280 µm | C (1,) 3 | -- " -- |
| $D^0$ | $4.3*10^{-13}$ | 130 µm | V2, 4 | -- " -- |
| $D^\pm_S$ ($F^\pm$) | $\approx 2.8*10^{-13}$ | $\approx$ 80 µm | C3, 5 | -- " -- |
| $\Lambda^0_c$ | $\approx 2.3*10^{-13}$ | $\approx$ 70 µm | C3, 5 | -- " -- |
| $\tau^\pm$ | $3.3*10^{-13}$ | 100 µm | C (1,) 3 | -- " -- |
| $T^0$, $T^\pm$ | $10^{-14}...10^{-15}$ | 0.3...3 µm | ? | excluded [4] |

(decay length $L = \eta*c*\tau$ with $\eta \equiv \beta\gamma = P/m$)

In conclusion, it will be desirable to gain a spatial resolution of a few 10 µm in the projection (x,y) normal to the magnetic field in order to identify decay vertices inside the beam tube. A still better spatial resolution (also in z) will be necessary for studies on lifetimes, angular distributions etc.

For charged one-prong decays ("kinks" C1), a geometrical vertex fit can only be performed if the vertex is well outside the beam tube; otherwise, the outgoing track will be flagged as "not associated". Decay topologies to be identified are V2...V6 for neutral and C3...C7 for charged decays.

Critical points are the following requirements

- from track search: reliable track element association, e.g. correct "hit merging" in the vertex detector [5];

- from global pattern recognition: reliable identification of decay vertices inside the tracking detectors.
- from single-track fitting: optimal precision of track parameters and their covariances at the reference cylinder (inner surface of the beam tube);

After a geometrical vertex fit, it is possible to re-adjust the fitted parameters using kinematic constraints in order to improve precision [6]. But beware of mistakes caused by wrong mass assignments or unmeasured (neutral) tracks.

The rest of this paper will present in more detail the algorithms for geometrical vertex fitting with emphasis on the Kalman filter method (chapter 1), strategies chosen for vertex evaluation in the DELPHI data analysis (chapter 2), and first results from a MC study on the precision of vertex fitting (chapter 3).

A convention generally used throughout this paper is to denote vectors by bold ($\mathbf{p}$), matrices by outlined ($\mathbb{C}$) symbols, and fitted estimates with a tilde ($\tilde{\mathbf{p}}$). Transposition of a matrix is denoted by superscript ($\mathbb{C}^T$), inversion by exponent ($\mathbb{C}^{-1}$). A distinction between column vectors ($\mathbf{p}$) and row vectors ($\mathbf{p}^T$) is made only when used in matrix operations.

This work was performed within the DELPHI Working Group on Data Analysis (chairman: Prof. J. Wickens, Brussels) and in contact with the DELPHI Vertex Detetector and Physics Analysis Groups. Special thanks are due to R. Frühwirth and Prof. M. Regler (Vienna) for their development of the basic algorithms and helpful collaboration.

# 1. Vertex Fitting and the Kalman Filter Method

The task of a geometrical single-vertex fit (for a given "bundle" of tracks) is to find an estimate for the vertex position $\tilde{\mathbf{x}}$ and for the track parameters $\tilde{\mathbf{q}}_i$ at the common vertex. This chapter will, after presenting the needed prerequisites, survey the algorithms for vertex fitting by different methods [7].

## 1.1 Prerequisites for Vertex Fitting [8,9]

The trajectory of a particle in space can be described by a set **p** of 5 parameters at some arbitrarily chosen reference surface (see below), e.g.

$\mathbf{p} = (R*\Phi,\ z,\ \theta,\ \phi,\ e/P)$ at R = const (cylinder), or
$\mathbf{p} = (\ x,\ \ y,\ \theta,\ \phi,\ e/P)$ at z = const (plane)

with $(R, \Phi, z)$ denoting a space point in cylindrical, $\mathbf{P} = (P, \theta, \phi)$ a momentum vector in spherical coordinates; e is the charge. The first two parameters define a point, the next two a direction at the reference surface. The 5th parameter is undefined in case of zero magnetic field **B**; otherwise, it is proportional to $\sin\theta'/r$, with $\theta'$ being the angle (**P**,**B**), and r the radius of curvature.

A track model is derived from the equations of motion of the particle and depends upon the characteristics of the magnetic field $\mathbf{B}(\mathbf{x})$. In case of a homogeneous field $\mathbf{B} = (0, 0, B_z)$, a helix track model will be appropriate.

In the absence of multiple scattering, the particle's trajectory is a deterministic result of "starting parameters" (**x**, **q**) at an arbitrary point. Therefore, making use of the track model, the track parameters **p** at a given reference surface can be expressed as a set of functions

$$\mathbf{p} = \mathbf{p}\,(\mathbf{x}, \mathbf{q})$$

with $\mathbf{x} = (x, y, z)$ being a point in space, and $\mathbf{q} = (\theta, \phi, e/P)$ the direction and (if defined) the inverse momentum at this point (fig. 1a). In the latter case, it may be useful to represent the momentum vector as $\mathbf{q} = (P_x, P_y, P_z)$ in cartesian coordinates (see section 1.5).

Single-track fitting yields, for each of n reconstructed tracks, a 5-vector of track parameters $\tilde{\mathbf{p}}_i$ and an associated 5x5 covariance matrix $\mathbb{G}_i^{-1}$, defined at some reference surface. For the single-vertex fit, these are now regarded as virtual measurements $\mathbf{p}_i$ with

$$\mathbf{p}_i = \tilde{\mathbf{p}}_i, \qquad \mathrm{cov}(\mathbf{p}_i,\mathbf{p}_i) \equiv \mathbb{G}_i^{-1} \qquad (i = 1 \ldots n)$$

Note the assumption $\mathrm{cov}(\mathbf{p}_i,\mathbf{p}_j) = 0$ for $i \neq j$ (this may be a subtle problem in detectors with bad multi-hit resolution, but affects pattern recognition rather than single-track fitting). The covariance (or error) matrix $\mathbb{G}_i^{-1}$ is symmetric, positive-definite with (in general) off-diagonal elements. Its inverse is the weight matrix $\mathbb{G}_i$.

A-priori knowledge of the position (with its errors) of the vertex, e.g. by measuring the beam spot, may be utilized in the vertex fit as another virtual measurement $\mathbf{v}$ and an associated (in most cases diagonal) 3x3 error matrix $\mathrm{cov}(\mathbf{v},\mathbf{v}) \equiv \mathbb{G}_0^{-1}$.

The $\mathbf{p}_i$ are assumed to be defined at a reference surface which has been chosen such that all errors coming from multiple scattering are included in $\mathbb{G}_i^{-1}$; this is the case if there is no significant matter between the vertex and the reference surface. E.g., when being interested in vertices inside the beam tube cylinder, its inner surface is a good choice.

If this condition is not fulfilled, $\mathbf{p}_i$ and $\mathbb{G}_i^{-1}$ must be propagated to a more inner reference surface while taking into account multiple scattering in the matter traversed, yielding $\mathbf{p}_i^*$ and $\mathbb{G}_i^{*-1}$. In case of the matter being concentrated in thin layers, these may easily be used step-by-step as new reference surfaces; for one such step (see fig. 1b),

$\mathbf{p}_i^* = \mathbf{p}_i^* (\mathbf{p}_i)$ defined by the track model
$\mathbb{D} \equiv \partial \mathbf{p}_i^* / \partial \mathbf{p}_i$ 5x5 matrix of derivatives (Jacobian)

Then one gets for the new covariance matrix

$$\mathbb{G}_i^{*-1} = \mathbb{D}\mathbb{G}_i^{-1}\mathbb{D}^T + \begin{Vmatrix} 0 & 0 & 0 & 0 & 0 \\ 0 & 0 & 0 & 0 & 0 \\ 0 & 0 & \sigma^2(\Delta\theta) & 0 & 0 \\ 0 & 0 & 0 & \sigma^2(\Delta\phi) & 0 \\ 0 & 0 & 0 & 0 & 0 \end{Vmatrix}$$

with the first term being the error propagation to the new reference surface, and the second term adding the errors from multiple scattering in that surface (using spherical coordinates $\theta$ and $\phi$). The latter, originating from a quasi-stochastic process, can be derived from Molière's formula, with logarithmic correction [3]

$$\sigma^2(\Delta\lambda) \approx \Delta s * (e*0.0141\ \text{GeV} / \beta*P)^2 * (1 + 0.111*\log_{10}\Delta s)^2$$

where $\Delta\lambda$ is the projection of the scattering angle into a plane containing the track direction, and $\Delta s$ is the track length in matter (in units of radiation length). Transformation to global spherical coordinates yields

$$\sigma^2(\Delta\theta) = \sigma^2(\Delta\lambda)$$
$$\sigma^2(\Delta\phi) = \sigma^2(\Delta\lambda) / \sin^2\theta$$

Noting that $\text{cov}(\Delta\theta,\Delta\phi) = 0$ gives the matrix elements shown above.

## 1.2 Vertex Fitting by the Least-Squares Method

The identity $\mathbf{v}(\mathbf{x}) = \mathbf{x}$ and a linear (1st order Taylor) ansatz for the n track model equations $\mathbf{p}_i(\mathbf{x},\mathbf{q}_i)$ around an arbitrarily chosen "expansion point" $(\mathbf{x}^0,\mathbf{q}_1{}^0,\ldots,\mathbf{q}_n{}^0)$ yield

$$\begin{Vmatrix} \mathbf{v} \\ \mathbf{p}_1 \\ \vdots \\ \mathbf{p}_n \end{Vmatrix} = \begin{Vmatrix} 1 & 0 & \ldots & 0 \\ \mathbb{A}_1 & \mathbb{B}_1 & \ldots & 0 \\ \vdots & \vdots & \ddots & \vdots \\ \mathbb{A}_n & 0 & \ldots & \mathbb{B}_n \end{Vmatrix} * \begin{Vmatrix} \mathbf{x} - \mathbf{x}^0 \\ \mathbf{q}_1 - \mathbf{q}_1{}^0 \\ \vdots \\ \mathbf{q}_n - \mathbf{q}_n{}^0 \end{Vmatrix} + \begin{Vmatrix} \mathbf{x}^0 \\ \mathbf{p}_1(\mathbf{x}^0,\mathbf{q}_1{}^0) \\ \vdots \\ \mathbf{p}_n(\mathbf{x}^0,\mathbf{q}_n{}^0) \end{Vmatrix}$$

with

$$\mathbb{A}_i \equiv \left[\partial\mathbf{p}_i / \partial\mathbf{x}\right]_{(\mathbf{x}^0,\mathbf{q}_i{}^0)} \qquad \mathbb{B}_i \equiv \left[\partial\mathbf{p}_i / \partial\mathbf{q}_i\right]_{(\mathbf{x}^0,\mathbf{q}_i{}^0)}$$

being 5x3 matrices composing the (5n+3)x(3n+3) matrix $\mathbb{M}$ of derivatives (Jacobian) at the expansion point.

It should be clear that it is not the track model equations $\mathbf{p}_i(\mathbf{x},\mathbf{q}_i)$ themselves which are linearized, but only the deviations $\mathbf{p}_i - \mathbf{p}_i(\mathbf{x}^0,\mathbf{q}_i{}^0)$ as functions of the deviations $(\mathbf{x}-\mathbf{x}^0, \mathbf{q}_i-\mathbf{q}_i{}^0)$ from the expansion point.

Note that the choice of an expansion point $(\mathbf{x}^0,\mathbf{q}_1{}^0,...,\mathbf{q}_n{}^0)$ is in principle arbitrary, nevertheless it should be chosen as close as "guessable" to the true values. E.g. for a primary vertex fit, the centre of the beam spot and the track parameters obtained by backward tracing are a good choice. If an expansion point is chosen too far away, i.e. the linear ansatz is no longer correct, several iterations will be needed for the fit, using the resulting estimates of one iteration as the expansion point for the next one.

The linear ansatz can be made homogeneous by re-defining the virtual measurements

$$\mathbf{p}_i \rightarrow \mathbf{p}_i' \equiv \mathbf{p}_i + \mathbb{A}_i\mathbf{x}^0 + \mathbb{B}_i\mathbf{q}_i{}^0 - \mathbf{p}_i(\mathbf{x}^0,\mathbf{q}_n{}^0)$$

to become "centred" around their expansion point values:

$$\begin{Vmatrix} \mathbf{v} \\ \mathbf{p}_1' \\ \vdots \\ \mathbf{p}_n' \end{Vmatrix} = \begin{Vmatrix} 1 & 0 & \cdots & 0 \\ \mathbb{A}_1 & \mathbb{B}_1 & \cdots & 0 \\ \vdots & \vdots & \ddots & \vdots \\ \mathbb{A}_n & 0 & \cdots & \mathbb{B}_n \end{Vmatrix} * \begin{Vmatrix} \mathbf{x} \\ \mathbf{q}_1 \\ \vdots \\ \mathbf{q}_n \end{Vmatrix}$$

This system of linear equations has 2n numbers of degrees of freedom (2n-3 if $\mathbb{G}_0 = 0$, i.e. there is no a-priori vertex measurement $\mathbf{v}$). Solutions for $(\mathbf{x},\mathbf{q}_1,...,\mathbf{q}_n)$ can be obtained by the least-squares method in a straightforward way:

$$\begin{Vmatrix} \tilde{\mathbf{x}} \\ \tilde{\mathbf{q}}_1 \\ \vdots \\ \tilde{\mathbf{q}}_n \end{Vmatrix} = (\mathbb{M}^T\mathbb{G}\mathbb{M})^{-1}\,\mathbb{M}^T\mathbb{G} * \begin{Vmatrix} \mathbf{v} \\ \mathbf{p}_1' \\ \vdots \\ \mathbf{p}_n' \end{Vmatrix}$$

with the Jacobian matrix $\mathbb{M}$ defined above, and the (5n+3)x(5n+3) weight matrix given by

$$\mathbb{G} = \begin{Vmatrix} \mathbb{G}_0 & & & \\ & \mathbb{G}_1 & & \\ & & \ddots & \\ & & & \mathbb{G}_n \end{Vmatrix}$$ with zeros off the block diagonal.

The (3n+3)x(3n+3) matrix $\mathbb{M}^T\mathbb{G}\mathbb{M}$ is the weight matrix of the vertex fit. The computing requirements are dominated by its inversion, with the number of arithmetic operations being proportional to $n^3$. If the vertex fit should also be used as a test criterium for the correct association of tracks, it must be repeated many times with different track combinations.

In conclusion, if the track multiplicity is high, or if there are ambiguities in track association, the straightforward method is prohibitive in practice.

A way out of this dilemma is to take advantage of the block structures of the matrices $\mathbb{M}$ and $\mathbb{G}$, which are a direct result of $\mathrm{cov}(\mathbf{p}_i,\mathbf{p}_j) = 0$ for $i \neq j$. This has first been suggested in ref. [10]. Further analysis of this problem has shown that its solution is equivalent to the linear filter method of Kalman [11,12].

## 1.3 Vertex Fitting by the Kalman Filter Method

The Kalman filter is an iterative algorithm for the addition (resp. removal) of a subset of (virtual) measurements to (resp. from) a linear least-squares fit. This is possible provided that all sub-sets are uncorrelated with each other.

For the application of this method to our vertex fit problem, we continue to follow the terminology and notation used so far. A mathematically more rigorous treatment is given in ref. [11]. We start with defining (2n+1) 3x3 matrices (note that $\mathbb{D}_i$ are unsymmetric):

$$\left.\begin{aligned} \mathbb{D}_0 &\equiv \mathbb{G}_0 + \sum \mathbb{A}_j^T \mathbb{G}_j \mathbb{A}_j \quad \text{(summation for } j = 1 \ldots n) \\ \mathbb{D}_i &\equiv \mathbb{A}_i^T \mathbb{G}_i \mathbb{B}_i \\ \mathbb{W}_i &\equiv (\mathbb{B}_i^T \mathbb{G}_i \mathbb{B}_i)^{-1} \end{aligned}\right\} \quad \text{for } i = 1 \ldots n$$

then we get for the covariances of the vertex position $\tilde{\mathbf{x}}$, the (3n+3)-vector of fitted parameters $(\tilde{\mathbf{x}}, \tilde{\mathbf{q}}_1, \ldots, \tilde{\mathbf{q}}_n)$ and the $\chi^2$ of the fit (summations for $j = 1 \ldots n$)

$$\mathrm{cov}(\tilde{\mathbf{x}},\tilde{\mathbf{x}}) \equiv \mathbb{C}_{00} = (\mathbb{D}_0 - \sum \mathbb{D}_j \mathbb{W}_j \mathbb{D}_j^T)^{-1}$$

$$\tilde{\mathbf{x}} = \mathbb{C}_{00} [\mathbb{G}_0 \mathbf{v} + \sum \mathbb{A}_j^T \mathbb{G}_j (1 - \mathbb{B}_j \mathbb{W}_j \mathbb{B}_j^T \mathbb{G}_j) \mathbf{p}_j']$$

$$\tilde{\mathbf{q}}_i = \mathbb{W}_i \mathbb{B}_i^T \mathbb{G}_i (- \mathbb{A}_i \tilde{\mathbf{x}} + \mathbf{p}_i') \qquad \text{for } i = 1 \ldots n$$

$$\chi^2 = (\mathbf{v} - \tilde{\mathbf{x}})^T \mathbb{G}_0 (\mathbf{v} - \tilde{\mathbf{x}}) + \sum (\mathbf{p}_j' - \tilde{\mathbf{p}}_j')^T \mathbb{G}_j (\mathbf{p}_j' - \tilde{\mathbf{p}}_j')$$

with

$$\tilde{\mathbf{p}}_j' \equiv \mathbf{p}_j'(\tilde{\mathbf{x}},\tilde{\mathbf{q}}_j) = \mathbb{A}_j\tilde{\mathbf{x}} + \mathbb{B}_j\tilde{\mathbf{q}}_j \qquad \text{(linear expansion of fitted values)}$$

It should be noted that these formulae contain an iterative algorithm by virtue of the summations; this will become manifest in the next section. The number of arithmetic operations required is only proportional to n, thus providing a fast algorithm. If the full covariance matrix of the vertex fit is also wanted (e.g. for a subsequent kinematics fit), we get

$$\begin{aligned}
\mathrm{cov}(\tilde{\mathbf{x}},\tilde{\mathbf{q}}_j) &\equiv \mathbb{C}_{0j} = -\,\mathbb{C}_{00}\,\mathbb{D}_j\,\mathbb{W}_j \\
\mathrm{cov}(\tilde{\mathbf{q}}_j,\tilde{\mathbf{x}}) &\equiv \mathbb{C}_{j0} = \mathbb{C}_{0j}^{\mathrm{T}} \\
\mathrm{cov}(\tilde{\mathbf{q}}_i,\tilde{\mathbf{q}}_j) &\equiv \mathbb{C}_{ij} = \delta_{ij}\,\mathbb{W}_j - \mathbb{W}_i\,\mathbb{D}_i^{\mathrm{T}}\,\mathbb{C}_{0j}
\end{aligned}$$

The number of arithmetic operations required is still proportional to n, except for $\mathrm{cov}(\tilde{\mathbf{q}}_i,\tilde{\mathbf{q}}_j)$ with $i \neq j$: in that case it is proportional to $n^2$. Comparing this with the straightforward method of the previous section (increase $\propto n^3$), a break-even is to be expected for vertices with ca. 4 tracks.

1.4 Method for Testing Track Association:

This is another benefit of the Kalman filter method, which follows from the iterative character of its algorithms. The problem to be solved is:

How do the results ($\tilde{\mathbf{x}}$, $\tilde{\mathbf{q}}_1$, ... , $\tilde{\mathbf{q}}_n$ and $\chi^2$) of a vertex fit with n tracks change, when either adding another track (n+1) to the fit, or removing one track ($k \leq n$) from the fit ? For track addition, we get

$$\begin{aligned}
\tilde{\mathbf{x}}^* &= \mathbb{C}_{00}^* \left[\mathbb{C}_{00}^{-1}\,\tilde{\mathbf{x}} + \mathbb{A}_{n+1}^{\mathrm{T}}\,\mathbb{G}_{n+1}\,(1 - \mathbb{B}_{n+1}\,\mathbb{W}_{n+1}\,\mathbb{B}_{n+1}^{\mathrm{T}}\,\mathbb{G}_{n+1})\,\mathbf{p}_{n+1}'\right] \\
\tilde{\mathbf{q}}_i^* &= \tilde{\mathbf{q}}_i - \mathbb{W}_i\,\mathbb{D}_i^{\mathrm{T}}\,(\tilde{\mathbf{x}}^* - \tilde{\mathbf{x}}) \qquad \text{for } i = 1 \ldots n \\
\tilde{\mathbf{q}}_{n+1}^* &= \mathbb{W}_{n+1}\,\mathbb{B}_{n+1}^{\mathrm{T}}\,\mathbb{G}_{n+1}\,(-\,\mathbb{A}_{n+1}\tilde{\mathbf{x}}^* + \mathbf{p}_{n+1}') \\
\chi^{2*} &= \chi^2 + (\tilde{\mathbf{x}} - \tilde{\mathbf{x}}^*)^{\mathrm{T}}\,\mathbb{C}_{00}^{-1}\,(\tilde{\mathbf{x}} - \tilde{\mathbf{x}}^*) + (\mathbf{p}_{n+1}' - \tilde{\mathbf{p}}_{n+1}^*)^{\mathrm{T}}\,\mathbb{G}_{n+1}\,(\mathbf{p}_{n+1}' - \tilde{\mathbf{p}}_{n+1}^*)
\end{aligned}$$

with

$$\begin{aligned}
\mathbb{C}_{00}^* &\equiv \left[\mathbb{C}_{00}^{-1} + \mathbb{A}_{n+1}^{\mathrm{T}}\,\mathbb{G}_{n+1}\,(1 - \mathbb{B}_{n+1}\,\mathbb{W}_{n+1}\,\mathbb{B}_{n+1}^{\mathrm{T}}\,\mathbb{G}_{n+1})\,\mathbb{A}_{n+1}\right]^{-1} \\
\tilde{\mathbf{p}}_{n+1}^* &\equiv \mathbf{p}_{n+1}'(\tilde{\mathbf{x}}^*,\tilde{\mathbf{q}}_{n+1}^*) = \mathbb{A}_{n+1}\tilde{\mathbf{x}}^* + \mathbb{B}_{n+1}\tilde{\mathbf{q}}_{n+1}^* \qquad \text{(linear expansion)}
\end{aligned}$$

For track removal, the same formulae can be used, with index (n+1) replaced by k, and changing sign of the matrices $\mathbb{G}_k$ and $\mathbb{W}_k$.

Defining the change in $\chi^2$ caused by the addition (resp. removal) of one track to (resp. from) the vertex fit as

$$\chi^2_+ \equiv \chi^{2*} - \chi^2 \geq 0 \qquad \text{(for addition of one track)}$$
$$\chi^2_- \equiv \chi^{2*} - \chi^2 \leq 0 \qquad \text{(for removal of one track)}$$

we can use $\chi^2_+$ or $\chi^2_-$ as a powerful test criterium for the correct association of a track to a vertex. In other words, wrongly associated tracks can be regarded as "outliers" with respect to the vertex fit [12].

Since $\chi^2_\pm$ incorporates all the information available (errors and covariances) of a fitted track to be tested, it is a more selective criterium than the usual method of testing impact parameters; this will be confirmed in chapter 3. Because the test can be performed one-by-one, there is no combinatorial overhead even in case of many ambiguous tracks. Therefore, $\chi^2_\pm$ is also a fast test criterium.

It should be noted, however, that the $\chi^2_\pm$ test is not absolutely selective either. It may fail to do a correct decision between competing vertices. These limits will be further investigated in chapter 3.

## 1.5 Inclusion of 3-momentum Conservation

The use of all 4 energy-momentum constraints at some vertex requires correct mass identification for the incoming and all outgoing particles. This is not always possible. For events with one or more secondary vertices, the kinematic constraints require a true multi-vertex fit to be performed.

Using only 3-momenta avoids the problem of unknown masses. The kinematic constraints are applied to only one secondary vertex; let's assume it is the decay of a particle coming from the primary vertex. Then following the Kalman filter method, the primary vertex position can be used as an additional virtual measurment $\mathbf{v}$ for the secondary vertex fit (fig. 1c). This requires only the inversion of a 7x7 matrix, and gives an update of the secondary vertex position $\tilde{\mathbf{x}}$ and the parameters for the connecting track $\tilde{\mathbf{Q}}$, together with a $\chi^2_+$ of the fit.

The $\chi^2_+$ can be used as a test criterium for the validity of the assumption above, i.e. to identify cascade decays. This is important for B meson physics.

## 2. Strategies for Vertex Evaluation in DELPHI

When speaking of "vertex evaluation", we have in mind a complex task which aims at achieving the following results:

- Identification of secondary vertices ("vertex separation");
- Association of reconstructed tracks to the identified vertices ("track bundling");
- Geometrical single-vertex fits, i.e. reconstruction of the position of all vertices and the parameters of all tracks at their vertex ("vertex fit");
- If needed, update of the vertex fits by the inclusion of kinematic constraints.

In this study, we are interested in vertex separation and track bundling only inside the beam tube. Outside, i.e. in regions covered by tracking detectors, these tasks will already have been done by global pattern recognition (PR), which should also be able to identify kinks.

In the framework of the DELPHI data analysis chain (DELANA), vertex evaluation will logically be performed after all charged tracks have been unambiguously reconstructed by single-track fitting. Since the reference surface is defined to be the inside of the beam tube cylinder, all multiple scattering is included in the error matrices (see section 1.1).

Our strategy adopted at present for vertex evaluation assumes event topologies with at least two primary vertex tracks which can be recognized a-priori (e.g. by their high momentum). These are used for a first approximate primary vertex fit. Then, all tracks are tested for their association to this vertex by the $|\chi^2_{\pm}|$ criterium (algorithms of section 1.4). This fast method should be able to associate a large fraction of all the primary vertex tracks.

Tracks which fail in the $|\chi^2_{\pm}|$ tests are subject to combinatorial bundling. It is this stage where secondary vertices (inside the beam tube) will be identified and the remaining tracks associated to a vertex. Developement of this part is also rather advanced [13] and it will soon be included in DELANA.

Finally, the primary vertex and all secondary vertices are fitted, using the algorithms of section 1.3. The same will be done for secondary vertices outside the beam tube which have been identified by global PR.

Later versions will allow to update the secondary vertex fits by the inclusion of 3-momentum conservation, either to improve the precision, or to identify cascade decays (see section 1.5). A simplified flow chart of our strategy being implemented in DELANA is given on the next page.

The assumption made above (existence of recognizable primary vertex tracks) is characteristic for the majority of $e^+e^-$ events at LEP energies, like the one shown in fig. 2 [14]. However, this is not the case for some event topologies which are of particular interest (e.g. $B\bar{B}$ production). For these, our strategy must be modified to allow for skipping the first approximate primary vertex fit and the fast track association tests. But, when relying only on combinatorial bundling without knowledge of a $|\chi^2_{\pm}|$, more sophisticated algorithms will be required.

Since the task of vertex identification and track bundling can be regarded as a problem of pattern recognition, it may be appropriate to solve it by using the principal components analysis (PCA) method [8]. The basic idea is to represent each pair of fitted tracks as one point in a 10-dimensional parameter space, with the similarity relation being that tracks originating from a common vertex must cross each other "very closely".

It should be sufficent to regard only the (x,y) projection normal to a (quasi)-homogeneous magnetic field **B**. Then, the feature pattern can be linearized by polar inversion, transforming circles of radius $r_H$ through the origin into straight lines with a distance of $1/r_H$ from the origin. Therefore, the sensitivity is fully kept for vertices near the origin, i.e. inside the beam tube. The 10-dimensional PCA transformation can be constructed from a carefully chosen training sample. The constraint hypersurface has in general 9 dimensions, but in our case effectively only 8 dimensions due to translation invariance in z.

The PCA method may also be used in place of combinatorial bundling after a first approximate vertex fit, as described above. The efficiency of its application will be investigated in another study to come.

The vertex evaluation package makes use of a utility library for helix tracking and error propagation (UHLIB) [15]. This library is field-proven and has become standard in the DELPHI data analysis.

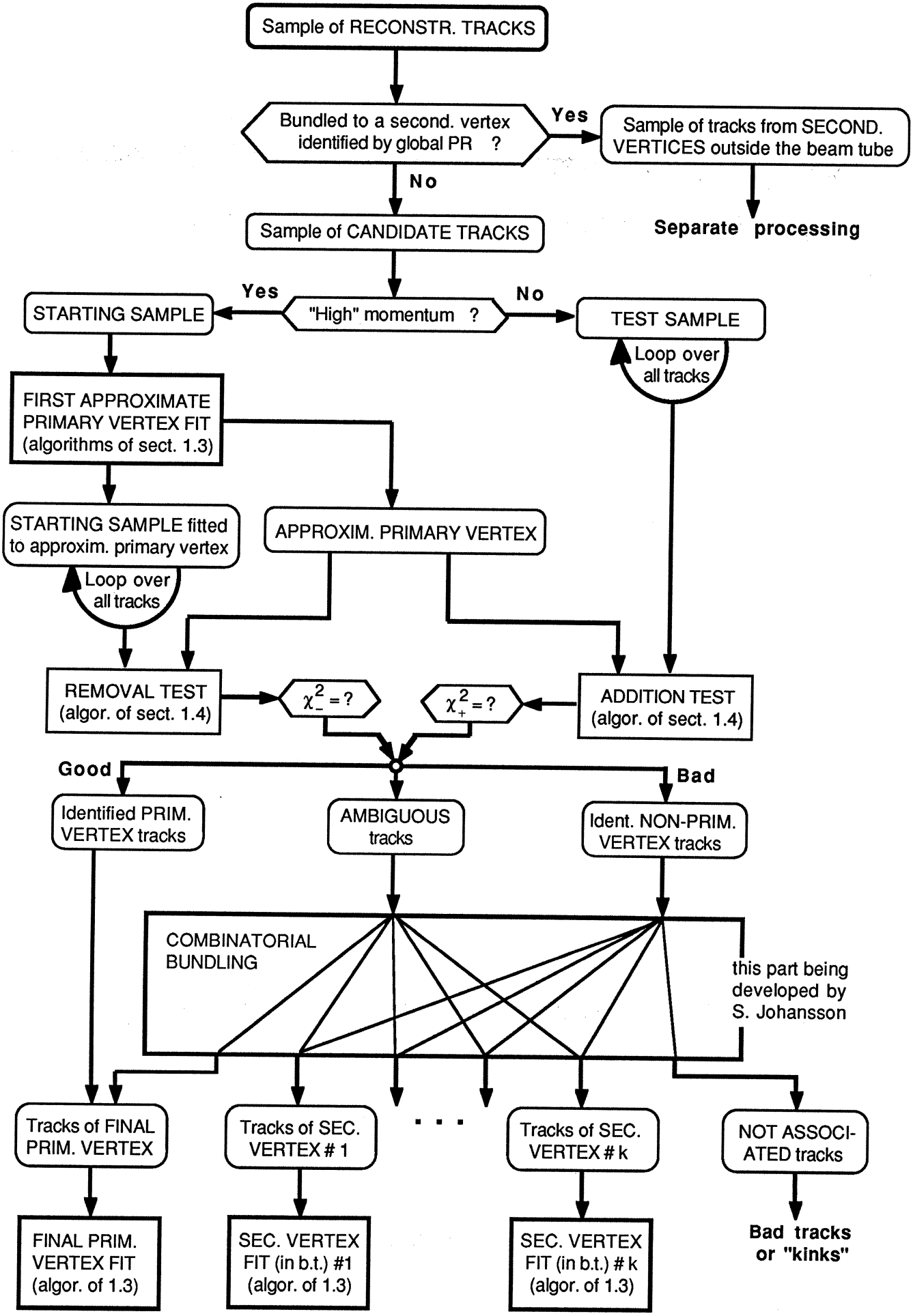
Sample of RECONSTR. TRACKS
Bundled to a second. vertex identified by global PR ?
Yes
Sample of tracks from SECOND. VERTICES outside the beam tube
Separate processing
No
Sample of CANDIDATE TRACKS
Yes
"High" momentum ?
No
STARTING SAMPLE
TEST SAMPLE
Loop over all tracks
FIRST APPROXIMATE PRIMARY VERTEX FIT (algorithms of sect. 1.3)
STARTING SAMPLE fitted to approxim. primary vertex
Loop over all tracks
APPROXIM. PRIMARY VERTEX
REMOVAL TEST (algor. of sect. 1.4)
$\chi^2_- = ?$
$\chi^2_+ = ?$
ADDITION TEST (algor. of sect. 1.4)
Good
Bad
Identified PRIM. VERTEX tracks
AMBIGUOUS tracks
Ident. NON-PRIM. VERTEX tracks
COMBINATORIAL BUNDLING
this part being developed by S. Johansson
Tracks of FINAL PRIM. VERTEX
Tracks of SEC. VERTEX # 1
Tracks of SEC. VERTEX # k
NOT ASSOCI-ATED tracks
FINAL PRIM. VERTEX FIT (algor. of 1.3)
SEC. VERTEX FIT (in b.t.) #1 (algor. of 1.3)
SEC. VERTEX FIT (in b.t.) # k (algor. of 1.3)
Bad tracks or "kinks"

## 3. Precision of the Vertex Fit (Monte-Carlo Study)

A warning from the very beginning: since the Monte-Carlo study is still going on, all results presented here are only preliminary (as of April 1988). Nevertheless, they elucidate some of the problems arising from our ambitious goals for vertex evaluation. This chapter will first describe a mini-simulation of and single-track fitting in the DELPHI spectrometer, and then discuss some aspects of primary vertex fitting and track association.

### 3.1 Mini-Simulation and Single-Track Fitting

The motivations for this work were twofold: first, to generate realistic virtual measurements (i.e. fitted tracks) to serve as input to the vertex fit procedures; second, to evaluate the effect of different detector set-ups on the precision of the track fit (Monte-Carlo study). These results have been published in more detail elsewhere [16].

The DELPHI spectrometer [2,5] is a complex set of individual detector modules (fig. 3a). Regarding the "barrel region" (fig. 3b), the following central tracking parts are considered for the mini-simulation: Beam Tube, 2 layers of Vertex Detector (VD), Inner Detector (ID) and Time Projection Chamber (TPC). All these parts are described by cylindrical surfaces around the z axis. A homogeneous magnetic field (1.2 T in the z direction) allows to use a helix track model. Multiple scattering is simulated using Molière's formula with logarithmic correction, and all matter assumed to be concentrated in thin layers.

Special care is taken to simulate fitted track segments with random errors as expected from measurements in the ID or TPC (error matrix with realistic off-diagonal elements). The VD returns only $R*\Phi$ measurements ($\sigma_{R\Phi} = 5$ μm, two-track resolution effects are not simulated). Constants used in the simulation for geometry, matter and measurement errors are quoted in ref. [16].

Using these simulated track segments as virtual measurements, a single-track fit is done by applying the Kalman filter method to track fitting: starting with the TPC and progressively moving inwards to the ID, layer 2 and layer 1 of the VD, up to the beam tube. This involves propagation of the (updated) parameter vector and error matrix to a new intermediate reference surface; inclusion of multiple

scattering effects to the error matrix, as described in section 1.1; and updating the fit (parameter vector $\tilde{\mathbf{p}}$ and error matrix $\mathbb{G}^{-1}$) by adding a new virtual measurement (fig. 3c). The final reference surface for the single-track fit is the inside of the beam tube cylinder ($R_{ref}$ = 8cm).

Fig. 4 shows some results of relevance for vertex fitting: the mean value of the impact parameters (obtained from the fitted $\tilde{\mathbf{p}}$) with respect to the known vertex, either in space or in the (x,y) projection, is plotted as a function of momentum and for different detector set-ups. It becomes clear that the VD adds accuracy only in the projection; this will help for the identification of short-lived decays, but not for determining lifetimes or angular distributions.

Knowing $\mathbf{p}^{true}$ at $R_{ref}$, the "normalized deviations" $(\tilde{\mathbf{p}} - \mathbf{p}^{true}) / \sqrt{var(\tilde{\mathbf{p}})}$ (with $var(\tilde{\mathbf{p}})$ being the diagonal of $\mathbb{G}^{-1}$) can be plotted for each of the 5 components of the parameter vector. They must be normally distributed with a mean = 0 and an r.m.s. = 1, thus constituting a very sensitive check for correctness.

## 3.2 Event Data Generated for the MC Study

At this early stage of the study, only "unphysical" data samples are used, which are sufficient for testing the most basic properties of the algorithms. The following discussions in this chapter are based upon 4 data samples:

**Sample A** of 200 events: primary vertex with 30 tracks, charge = ±1 (equally)
P = 2 ... 22 GeV/c (flat distribution)
cotθ = −1 ... +1 -- " --
$\phi$ = 0 ... 2$\pi$ -- " --

**Sample B** of 100 events: primary vertex with 20 tracks, kinematics as above;
4 secondary vertices: $P_{decay}$ = 10 GeV/c
$m_{decay}$ = 1.86 GeV (≙ $D^0$ mass)
isotropic decays into $K^-\pi^+\pi^-$, $K^+\pi^-\pi^+$, $K^-\pi^+$, $K^+\pi^-$
decay lengths = 800 μm (in the laboratory system)

**Sample C** of 100 events: as sample B, but decay lengths = 2400 μm

**Sample D** of 100 events: as sample B, but $P_{decay}$ = 5 ... 10 GeV/c (flat distr.)
$m_{decay}$ = 5.275 GeV (≙ $B^0$ mass)

Sample A is supposed to test the quality of a "clean" primary vertex fit with high track multiplicity. Samples B ... D are supposed to test, after an approximate primary vertex fit, the association of "right" and "wrong" tracks for different kinds of the latter. It may be expected that samples C (longer decay lengths) and D (lower momenta and higher masses) will enable better selection than sample B.

These data samples are passed through the mini-simulation and single-track fitting program described in section 3.1, considering only tracks with $|\cot\theta| \leq 1$ (i.e. those passing through the VD). The impact parameters in space resp. in (x,y) projection, w.r. to the vertex, are shown in figs. 9 ... 12 for samples A ... D.

### 3.3 Primary Vertex Fit and Track Association

The processing follows the procedures described in chapter 2, making use of the algorithms given in sections 1.3 and 1.4. Tracks of the "starting sample" for a first approximate primary vertex fit are selected by $P \geq P_{cut} = 10$ GeV/c.

The $\chi^2_+$ (addition) test is performed for all tracks of the "test sample" ($P < P_{cut}$), and the $\chi^2_-$ (removal) test for all tracks of the "starting sample" ($P \geq P_{cut}$). These $\chi^2_\pm$ tests are performed without updating the results of the first approximate primary vertex fit.

Selection of tracks for the final primary vertex fit: For data sample A, the $\chi^2_\pm$ are ignored, i.e. all tracks are selected. For data samples B ... D, tracks are selected by the $\chi^2_\pm$ test with $|\chi^2_\pm| \leq |\chi^2_\pm|_{cut} = 3$, corresponding to a loss of ca. 22% of "good" tracks. It should be clear that such a tight cut is chosen here for test purposes only.

As with the single-track fit, a very sensitive check for correctness can be performed for simulated data because of knowing $(\mathbf{x}^{true}, \mathbf{q}_1{}^{true}, ..., \mathbf{q}_n{}^{true})$ at the vertex. Plotting the "normalized deviations" for each component of

$$(\tilde{\mathbf{x}} - \mathbf{x}^{true}) / \sqrt{var(\tilde{\mathbf{x}})} \qquad \text{with } var(\tilde{\mathbf{x}}) = \mathbf{diag}(\mathbb{C}_{00}) \qquad \text{and}$$

$$(\tilde{\mathbf{q}}_i - \mathbf{q}_i{}^{true}) / \sqrt{var(\tilde{\mathbf{q}}_i)} \qquad \text{with } var(\tilde{\mathbf{q}}_i) = \mathbf{diag}(\mathbb{C}_{ii}) \qquad \text{for } i = 1 ... n$$

must result in normal distributions with a mean = 0 and an r.m.s. = 1. Correct input from the single-track fit is, of course, obligatory.

Further checks for correctness involve the $\chi^2$ of a vertex fit resp. the $|\chi^2_\pm|$ of track association tests. Both must be $\chi^2$-distributed, i.e. have a mean = NDF and an r.m.s. = $\sqrt{2*NDF}$, with NDF being the number of degrees of freedom.

In case of a vertex fit with n tracks, NDF = 2n (or 2n-3 if not using the beam spot); therefore, plotting $\chi^2$/NDF gives a mean = 1. In case of track association tests, NDF = 2, so plots of $|\chi^2_\pm|$ are $\chi^2$-distributed with a mean = 2 and an r.m.s. = 2; this can be seen in figs. 5 and 6,7,8:a,c.

It should be noted, however, that these checks are only fulfilled if the tracks are fitted to their correct vertex. E.g., when testing association of "wrong" tracks to the primary vertex, the $|\chi^2_\pm|$ of the test are no $\chi^2$-distribution anymore (figs. 6,7,8:b). Similarly, when losing too many "good" tracks after a tight $|\chi^2_\pm|$ cut, the $\chi^2$/NDF distribution of the final vertex fit will also be distorted (mean < 1).

## 3.4 Preliminary Results of the Primary Vertex Fit

The precision of a primary vertex fit may be defined by the deviations of the fitted parameters $(\tilde{\mathbf{x}}, \tilde{\mathbf{q}}_1, \ldots, \tilde{\mathbf{q}}_n)$ with respect to the true ones $(\mathbf{x}^{true}, \mathbf{q}_1{}^{true}, \ldots, \mathbf{q}_n{}^{true})$,

$$\Delta\mathbf{x} \equiv (\Delta x, \Delta y, \Delta z) = (\tilde{\mathbf{x}} - \mathbf{x}^{true})$$
$$\Delta\mathbf{q}_i \equiv (\Delta\theta_i, \Delta\phi_i, \Delta(\tfrac{q}{p})_i) = (\tilde{\mathbf{q}}_i - \mathbf{q}_i{}^{true}) \qquad \text{with } i = 1 \ldots n$$

Plotting these for each component results in distributions with a mean = 0 and an r.m.s. to be determined, as shown in the following table:

| Data sample | A | B | C | D |
|---|---|---|---|---|
| no. of events | 200 | 100 | 100 | 99 |
| no. of tracks for pr. vx. fit | 5997 | 1817 | 1631 | 1573 |
| mean (tracks / ev.) -- " -- | 30.0 | 18.2 | 16.3 | 15.9 |
| r.m.s. ($\Delta x$) / $\mu$m | 5.90 | 8.04 | 7.54 | 7.99 |
| r.m.s. ($\Delta y$) / $\mu$m | 6.12 | 8.21 | 8.24 | 7.59 |
| r.m.s. ($\Delta z$) / $\mu$m | 37.8 | 50.3 | 53.0 | 54.8 |
| r.m.s. ($\Delta\theta_i$) / mrad | 0.325 | 0.340 | 0.328 | 0.336 |
| r.m.s. ($\Delta\phi_i$) / mrad | 0.091 | 0.134 | 0.117 | 0.113 |
| r.m.s. ($\Delta(\frac{q}{p})_i$) / GeV$^{-1}$ | 0.0015 | 0.0015 | 0.0014 | 0.0014 |

Regarding $\Delta x$, $\Delta y$ and $\Delta z$, the higher precision of sample A is mainly due to the higher number of tracks entering the vertex fit.

Comparing, for sample A, the mean values of the impact parameter, either in space (fig. 9a) or in (x,y) projection (fig. 9b), with the quadratically added r.m.s. of the vertex position (see table above) shows clearly the gain in precision resulting from fitting many tracks to a common vertex:

| | |
|---|---|
| mean (impact parameter in space) | 153.7 μm |
| r.m.s. $\left(\sqrt{\Delta x^2+\Delta y^2+\Delta z^2}\right)$ | 38.7 μm |
| mean (impact parameter proj. to (x,y)) | 23.5 μm |
| r.m.s. $\left(\sqrt{\Delta x^2+\Delta y^2}\right)$ | 8.5 μm |

It should not be forgotten, however, that these values represent the "ideal case": high track multiplicity, no ambiguities from pattern recognition, no ambiguities from track association. Therefore, they give an indication for the optimal precision achievable rather than for a realistic one to be expected.

## 3.5 Preliminary Results of Track Association

In order to evaluate the selection power of the $\chi^2_\pm$ test described in section 1.4, we plot for data samples B (fig. 6), C (fig. 7) and D (fig. 8) the $\chi^2_+$ (addition test) for primary vertex tracks (figs. *:a), the $\chi^2_+$ (addition test) for secondary vertex tracks (figs. *:b), and the $|\chi^2_-|$ (removal test) for primary vertex tracks (figs. *:c). The $|\chi^2_-|$ (removal test) for secondary vertex tracks is not shown because almost none of these have momenta $P \geq P_{cut} = 10$ GeV/c.

Whereas the $|\chi^2_\pm|$ are "correctly" distributed (mean = r.m.s. = 2) for primary vertex tracks (figs. *:a,c), this is not the case for the $\chi^2_+$ of "wrong" (secondary vertex) tracks, which have mean and r.m.s. $\approx$ 5 for data sample B (fig. 6b), and even much bigger for data samples C (fig. 7b) and D (fig. 8b).

A comparison of the $\chi^2_+$ distributions for "right" tracks (figs. *:a) with the corresponding ones for "wrong" tracks (figs. *:b) shows that also the latter do not decrease at lowest values. As a consequence, any selection criterium based exclusively upon $\chi^2_\pm$ cuts has to find a compromise between too much losses and too much contamination.

Choosing a rather tight cut at $|\chi^2_{\pm}| \leq |\chi^2_{\pm}|_{cut} = 3$ gives, for the particular cases of our data samples, the following percentages for losses of "right" resp. contamination with "wrong" tracks:

| Data sample | B | C | D |
|---|---|---|---|
| losses by $\chi^2_+$ and $\chi^2_-$ tests [%] | 22 | 22 | 23 |
| contamination by $\chi^2_+$ tests [%] | 13 | 3.5 | 2 |

It is clear that, for a fixed $|\chi^2_{\pm}|_{cut} = 3$, the losses are constantly $\approx$ 22 %. The contamination from "wrong" tracks is smaller; it decreases as the $\chi^2_+$ distributions get more and more distorted towards high values for data samples B - C - D.

3.6 Comparison with Impact Parameter Tests

Given the same conditions, which is the selection power of the usually performed impact parameter tests? For this aim, we plot for our data samples B (fig. 10), C (fig. 11) and D (fig. 12) the impact parameters in space (figs. *:a,b) resp. in (x,y) projection (figs. *:c,d), with respect to the true primary vertex, for "right" (primary vertex) tracks (figs. *:a,c) and "wrong" (secondary vertex) tracks (figs. *:b,d).

Comparing the corresponding distributions for "right" and "wrong" tracks show that for the impact parameters in space there is a bigger overlap (worse selectivity) than for the projected impact parameters. In both cases, a high percentage of contamination is to be expected.

Performing cuts on the impact parameters at such values that the percentage of losses of "right" tracks is the same as with the $\chi^2_{\pm}$ cuts applied above, the resulting contamination with "wrong" tracks will be

| Data sample | B | C | D |
|---|---|---|---|
| losses (see above) [%] | 22 | 22 | 23 |
| contamination by I.P. i. space cuts [%] | 32 | 23 | 16 |
| contamination by I.P. project. cuts [%] | 22 | 9 | 5 |

which is no surprise. But it is clear that $\chi^2_{\pm}$ tests constitute a more powerful selection criterium than any of the impact parameter tests. Thus, our expectations of section 1.4 are confirmed.

## 3.7 Preliminary Conclusions and Outlook

The Kalman filter method (in its general and rigorous form) is used for the first time in a real computer program for fitting vertices and testing track association in a storage ring experiment. It has been shown to work fast and reliably. The part of the program doing a geometrical primary vertex fit (with all tracks) is already included in the DELPHI data analysis chain.

How powerful is the $\chi^2_{\pm}$ as a test criterium for track association to the primary vertex? The method has been shown to be superior to the usual impact parameter tests. But for short-lived decays (like B and D mesons), it is still not as selective as wanted.

Therefore, the method needs still a lot of study in order to develop more sophisticated test criteria. Suggested are tests combining the $\chi^2_{\pm}$ with other relevant criteria, like the momentum P of the track, or the $\chi^2$ of a fitted "candidate" secondary vertex. It may turn out necessary to have different test criteria for different physics channels of interest, each being highly selective for the own channel, but possibly bad for the others.

In any case, there will remain a region of ambiguity, which can only be treated by combinatorial bundling. After the association of all primary vertex tracks, combinatorial bundling will also be necessary for distributing the remaining tracks among the secondary vertices, which thus become identified. (Application of the PCA method for this task will be investigated in another study to come.) After the correct bundling of all tracks, the geometrical secondary vertex fit uses the same algorithms as the primary vertex fit.

Due to the vertex detector, the precision of the fitted vertex position is rather bad in the z coordinate (see table in section 3.4). A way to correct this drawback would be to re-adjust the fitted vertex parameters using kinematics information, with the danger of possible distortions caused by wrong mass assignements.

This may be avoided by using only 3-momentum constraints. Application of the method outlined in section 1.5 for the identification of cascade decays of B mesons will be part of another study to come.

## References


[1] J. Ellis and R. Peccei (editors): Physics at LEP. CERN **86-02** (2 vols.).

[2] DELPHI Technical Proposal. DELPHI **83-66**/1.
DELPHI Progress Report. DELPHI **84-60**/GEN-11.

[3] M. Aguilar-Benitez et al.: Review of Particle Properties. Phys.Lett. **170B** (1986).

[4] M. Klein, H. Pietschmann and H. Rupertsberger: On the Decay of the Top-Quark. Phys.Lett. **153B** (1985) 341.

[5] G. Anzivino et al.: DELPHI Microvertex Detector. DELPHI **86-86**/GEN-52.

[6] G.E. Forden and D.H. Saxon: Improving Vertex Position Determination by Using a Kinematic Fit. Nucl.Instr.Meth. **A248** (1986) 439 [RAL-**85-037**].

[7] P. Billoir, R. Frühwirth and M. Regler: Track Element Merging Strategy and Vertex Fitting in Complex Modular Detectors. Nucl.Instr.Meth. **A241** (1985) 115 [DELPHI **85-26**/PROG-21].

[8] R. Frühwirth and M. Regler: Reconstruction of Charged Particle Trajectories. Proc. Advanced Study Inst. on Techniques and Concepts in HEP, St. Croix (Virgin Islands), July 1988. Plenum Publ. Corp. (Univ. of Rochester, NY).

[9] R. Böck, H. Grote, D. Notz and M. Regler: Data Analysis Techniques in High Energy Physics Experiments. Cambridge University Press, 1988.

[10] M. Metcalf, M. Regler and C. Broll: A Split Field Magnet Geometry Fit Program - NICOLE. CERN **73-2**.

[11] R. Frühwirth: Application of Kalman Filtering to Track and Vertex Fitting. Nucl.Instr.Meth. **A262** (1987) 444 [DELPHI **87-23**/PROG-70].

[12] R. Frühwirth: Thesis. Technische Universität, Vienna, 1988.

[13] S. Johansson (CERN, Div. EP): private communication.

[14] W.T. Ford: B Physics in $e^+e^-$ Colliders Far Above Threshold. Proc. of this Conf.

[15] W.A. Mitaroff: Status of Utility Library for Helix Tracking and Error Propagation. DELPHI **87-51**/PROG-85.

[16] P. Billoir, Ph. Herquet, W.A. Mitaroff, M. Regler and J. Wickens: Report on Global Track and Vertex Fitting in the DELPHI Detector. DELPHI **86-99**/PROG-61.

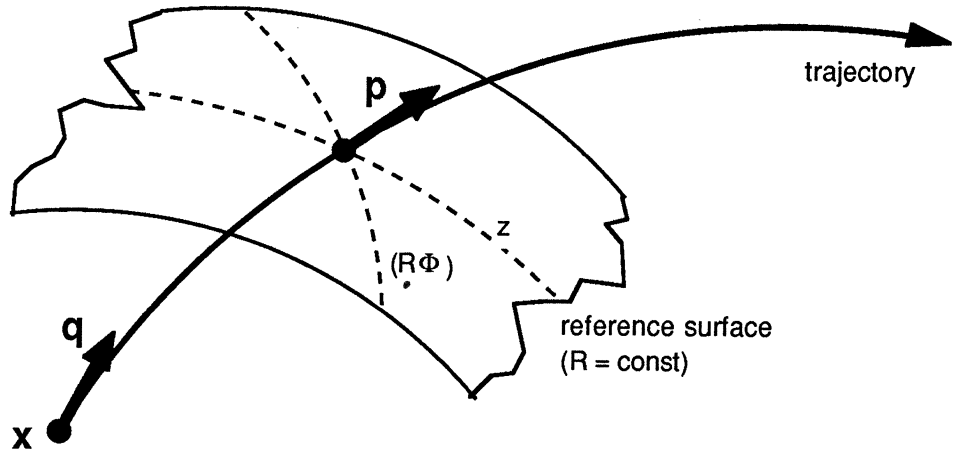


**Fig. 1a** Definition of a track model

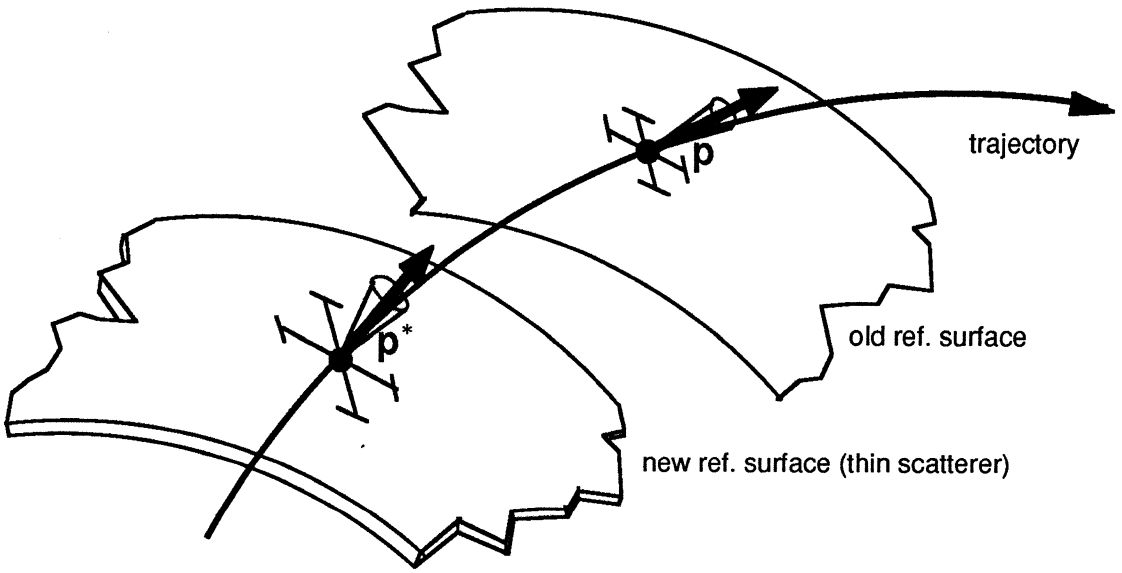


**Fig. 1b** One step of error propagation

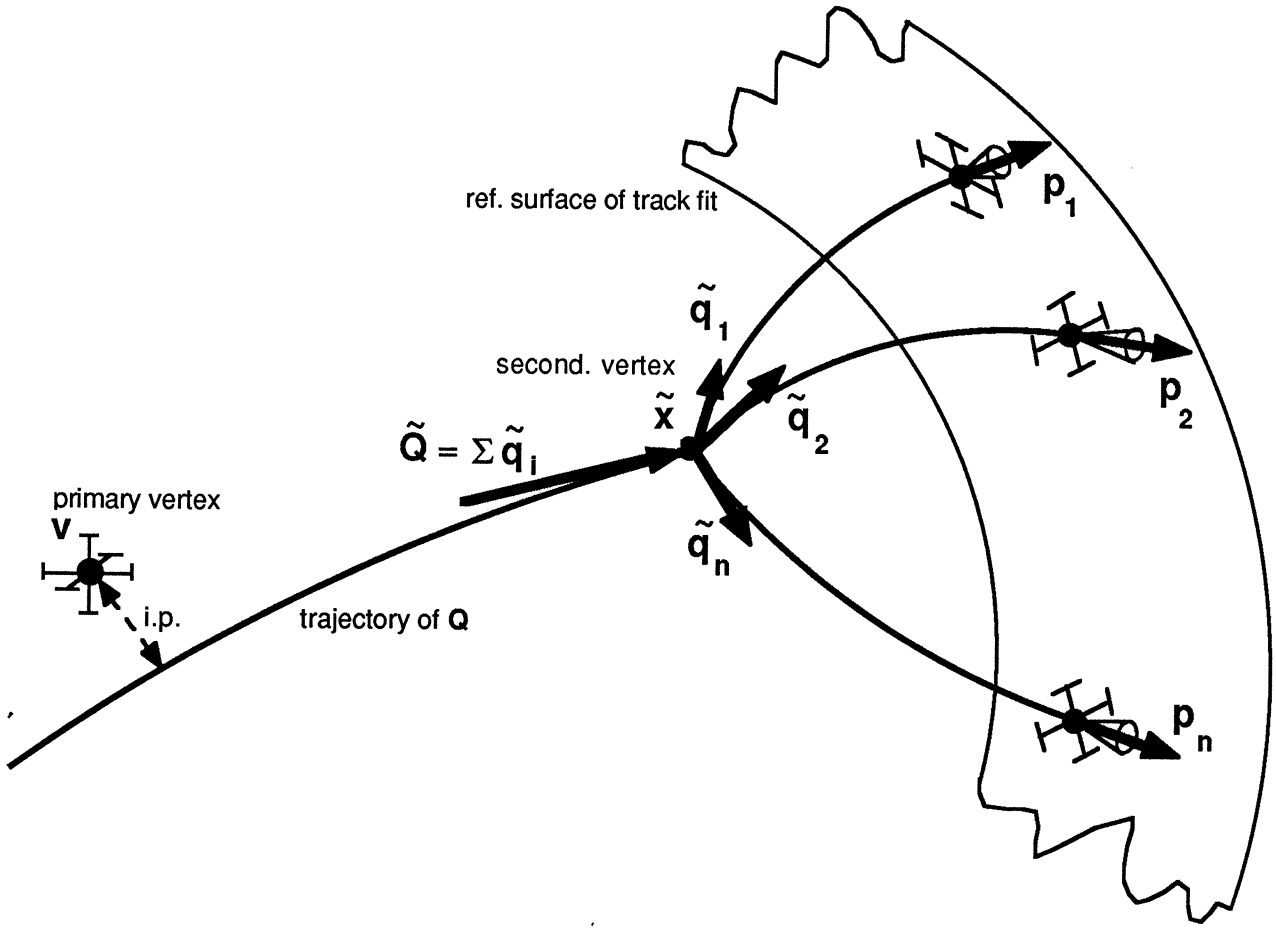


**Fig. 1c** Update of a secondary vertex fit by the inclusion of 3-momentum conservation

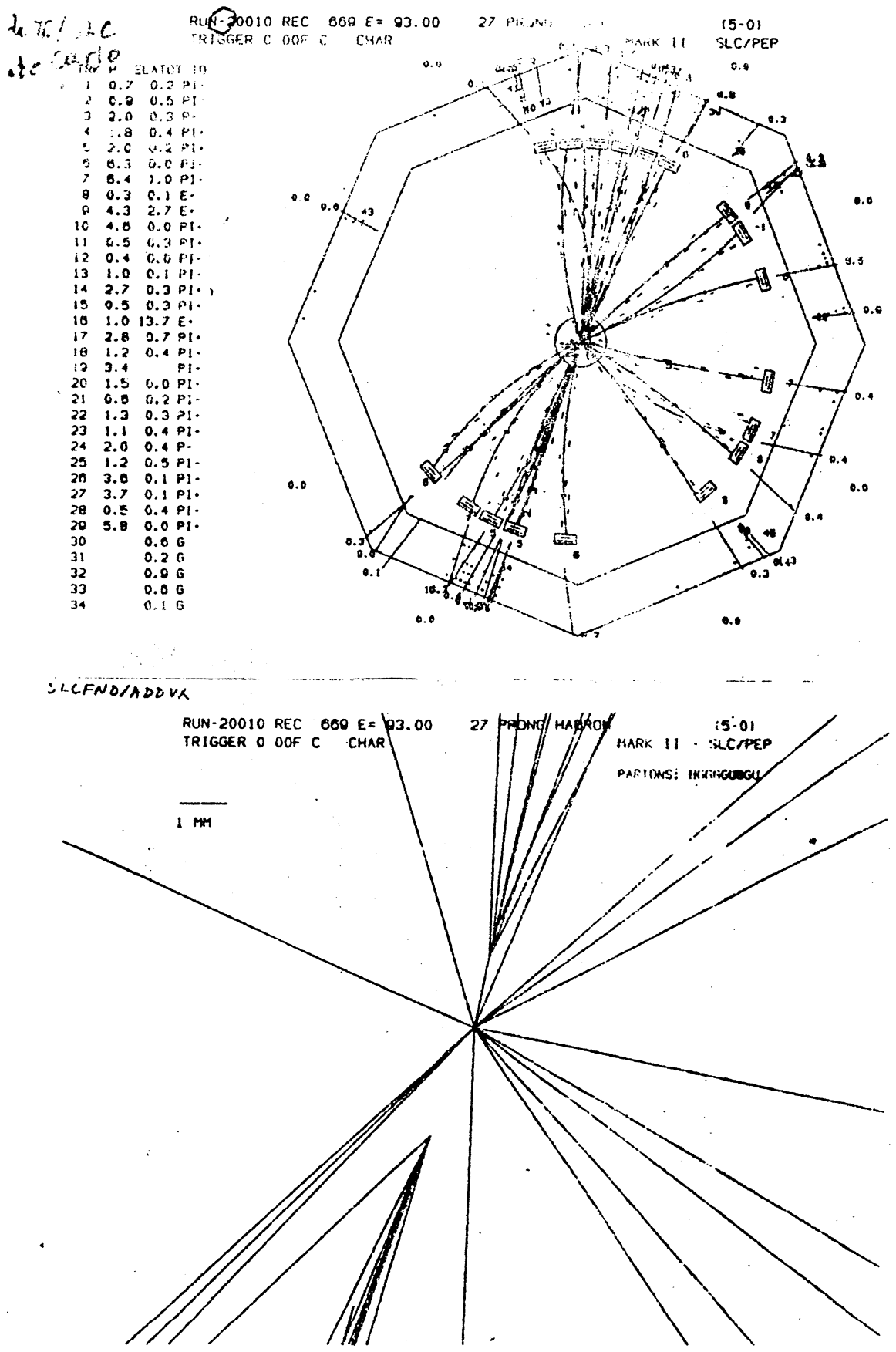


**Fig. 2** Typical hadronic event (E = 93 GeV), simulated for SLC - Mark II
(by courtesy of Prof. W. T. Ford, Univ. of Colorado)

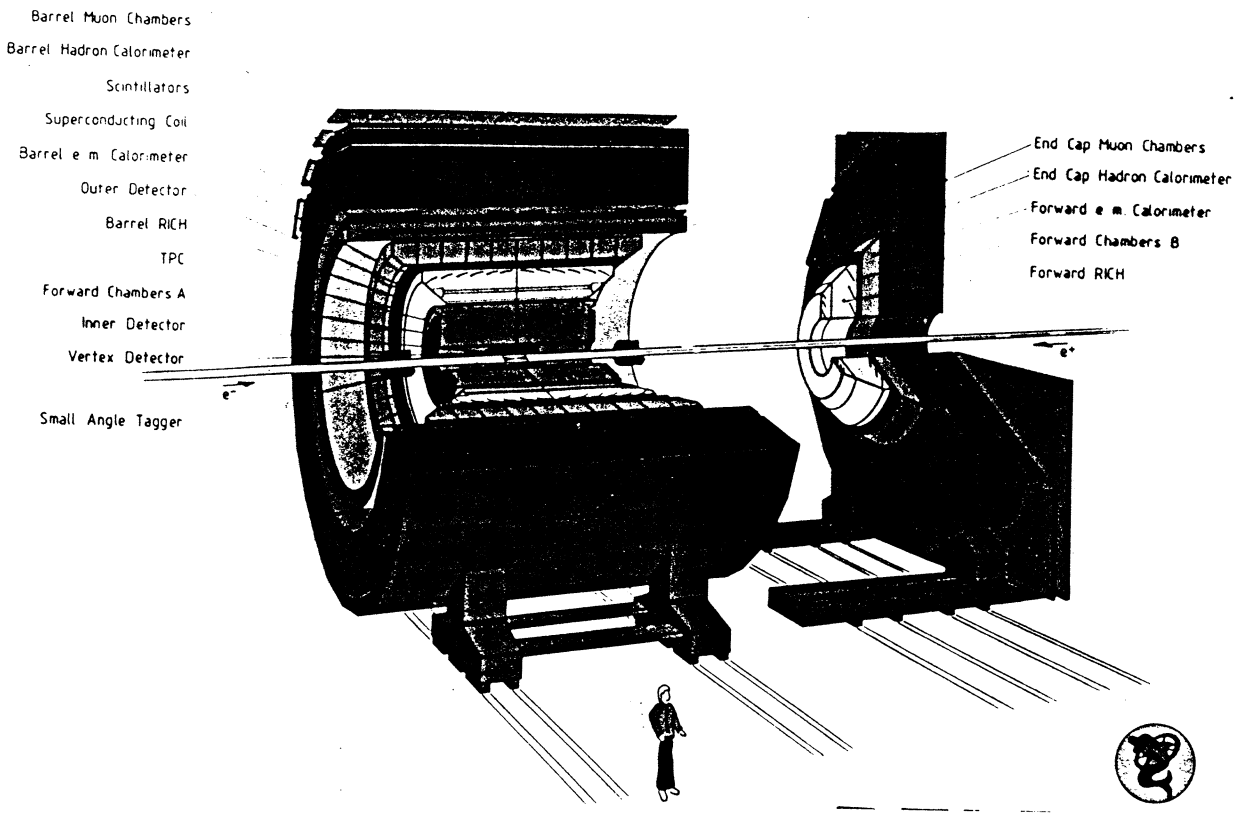


**Fig. 3a** The DELPHI spectrometer (schematic view)

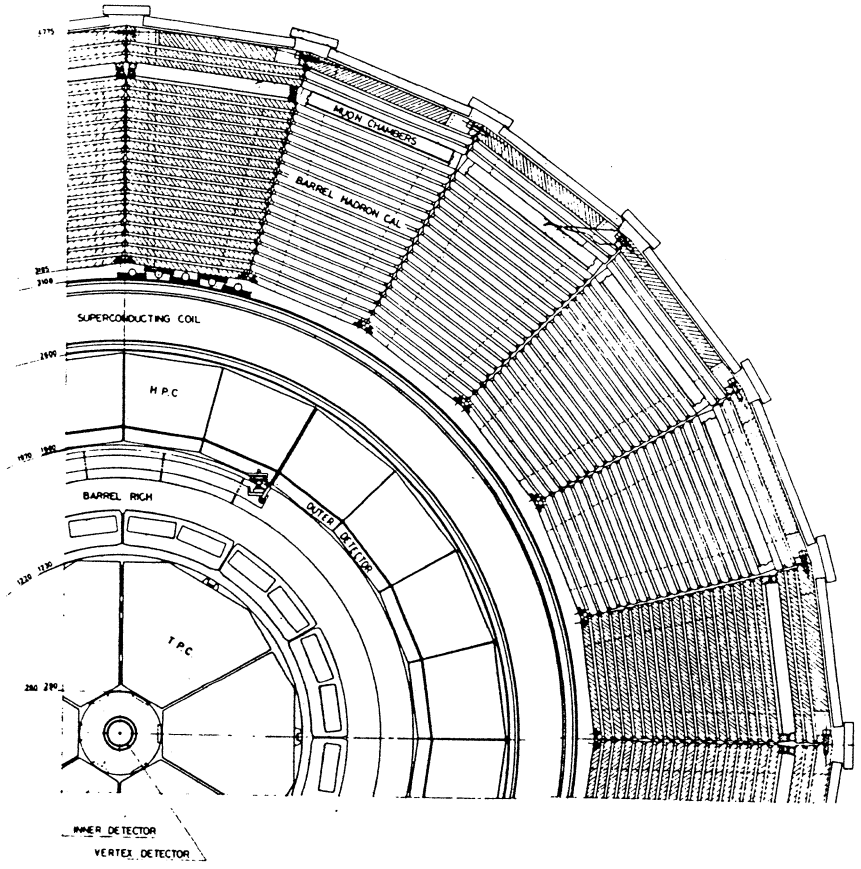


**Fig. 3b** Transverse section of the DELPHI spectrometer

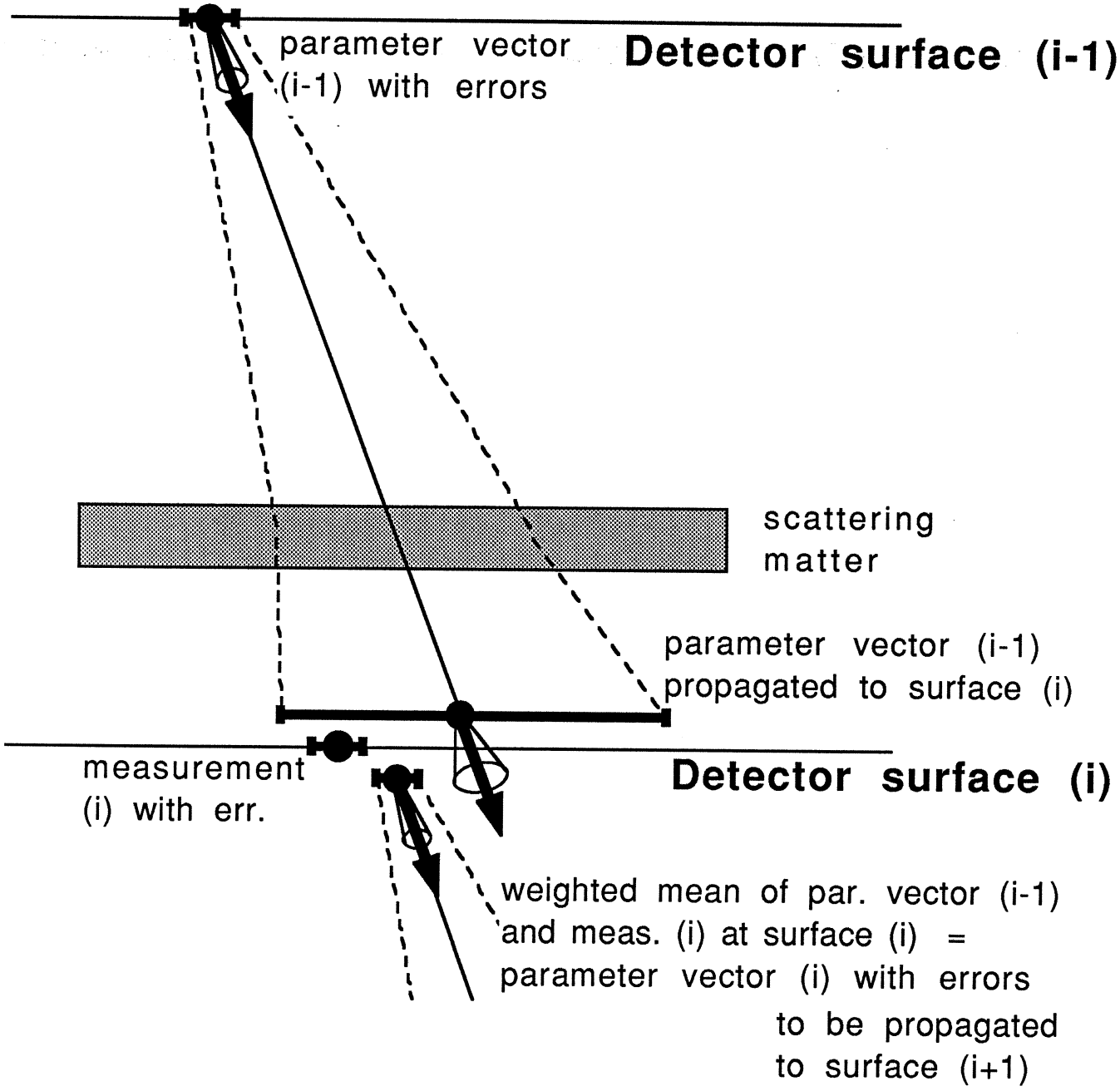


**Fig. 3c** One step of single-track fitting by the Kalman filter method
(by courtesy of Cambridge University Press)

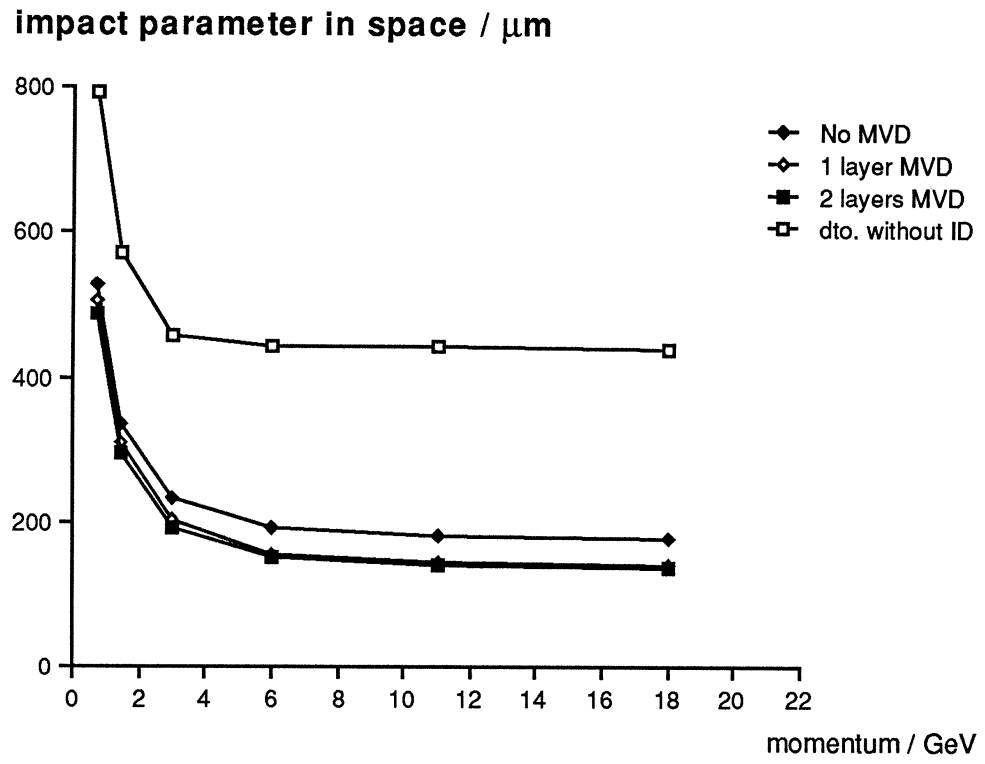


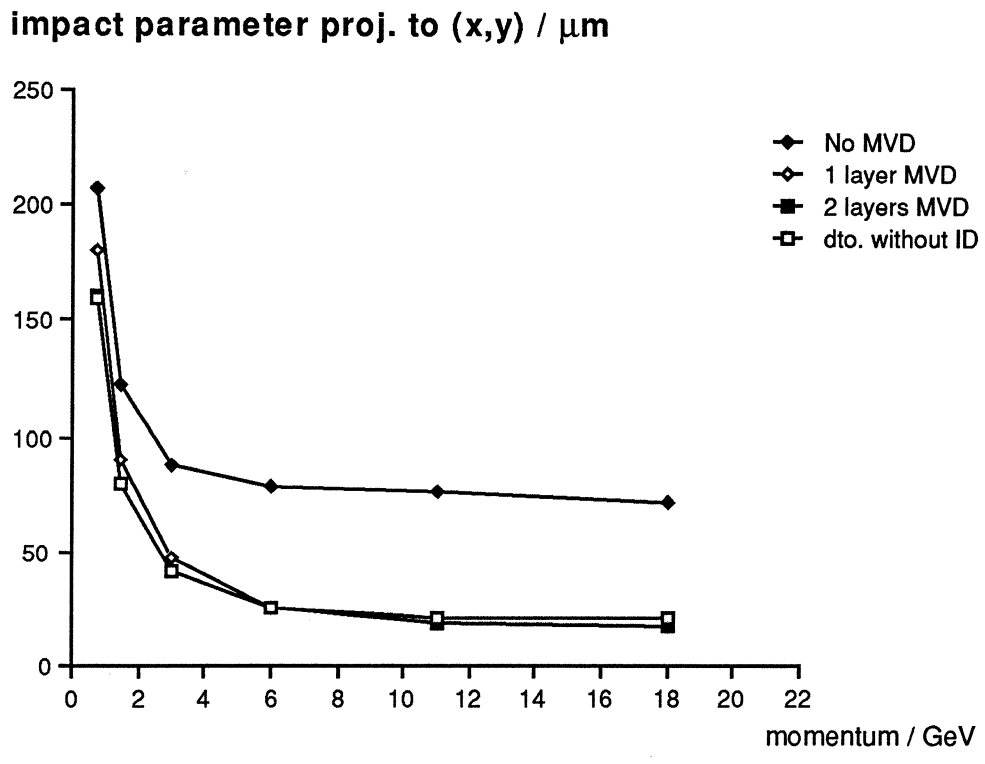


**Fig. 4** Precision of Single-Track Fitting (MC Data)

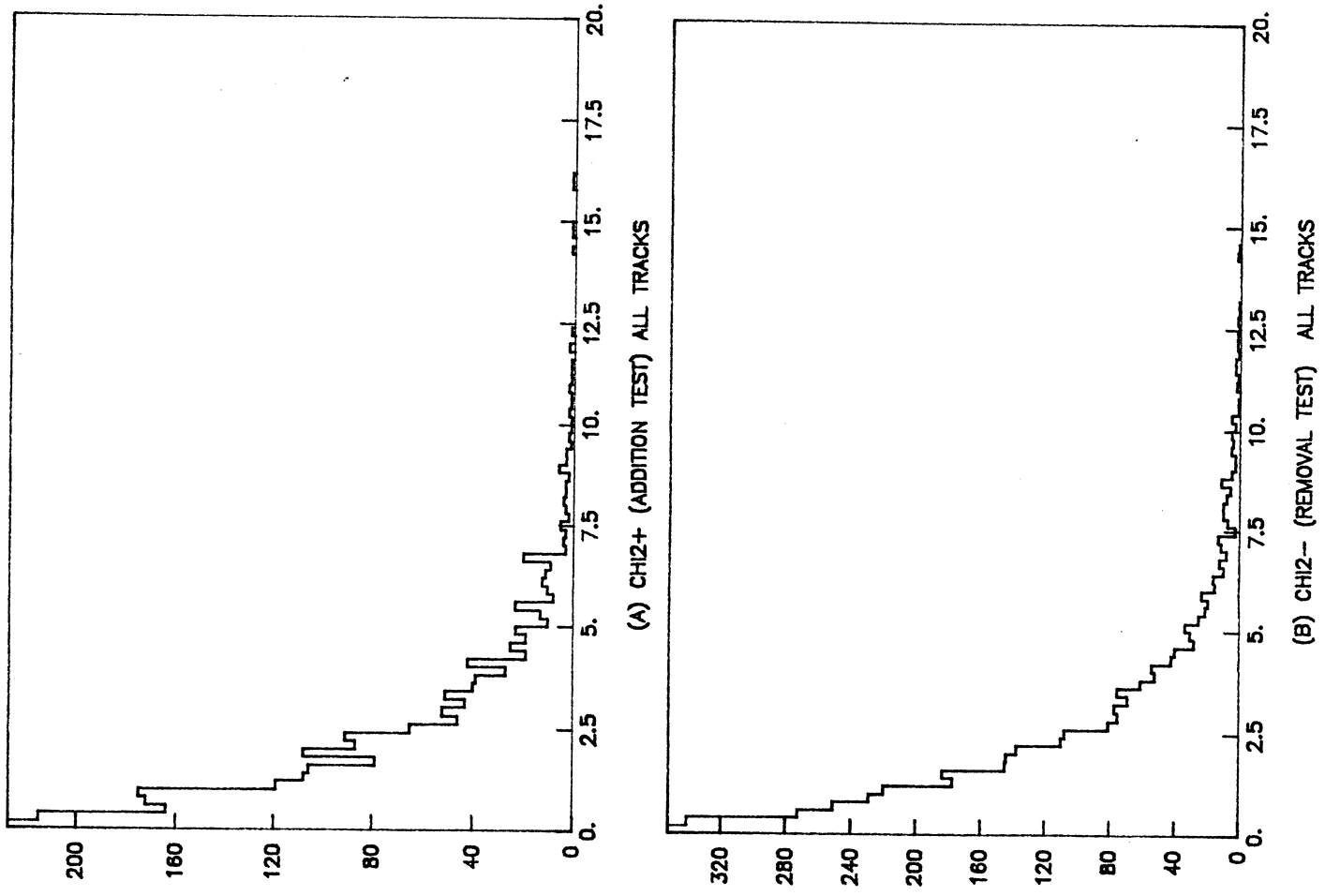


**Fig. 5** Testing track association to primary vertex: $|\chi^2_{\pm}|$ for data sample A

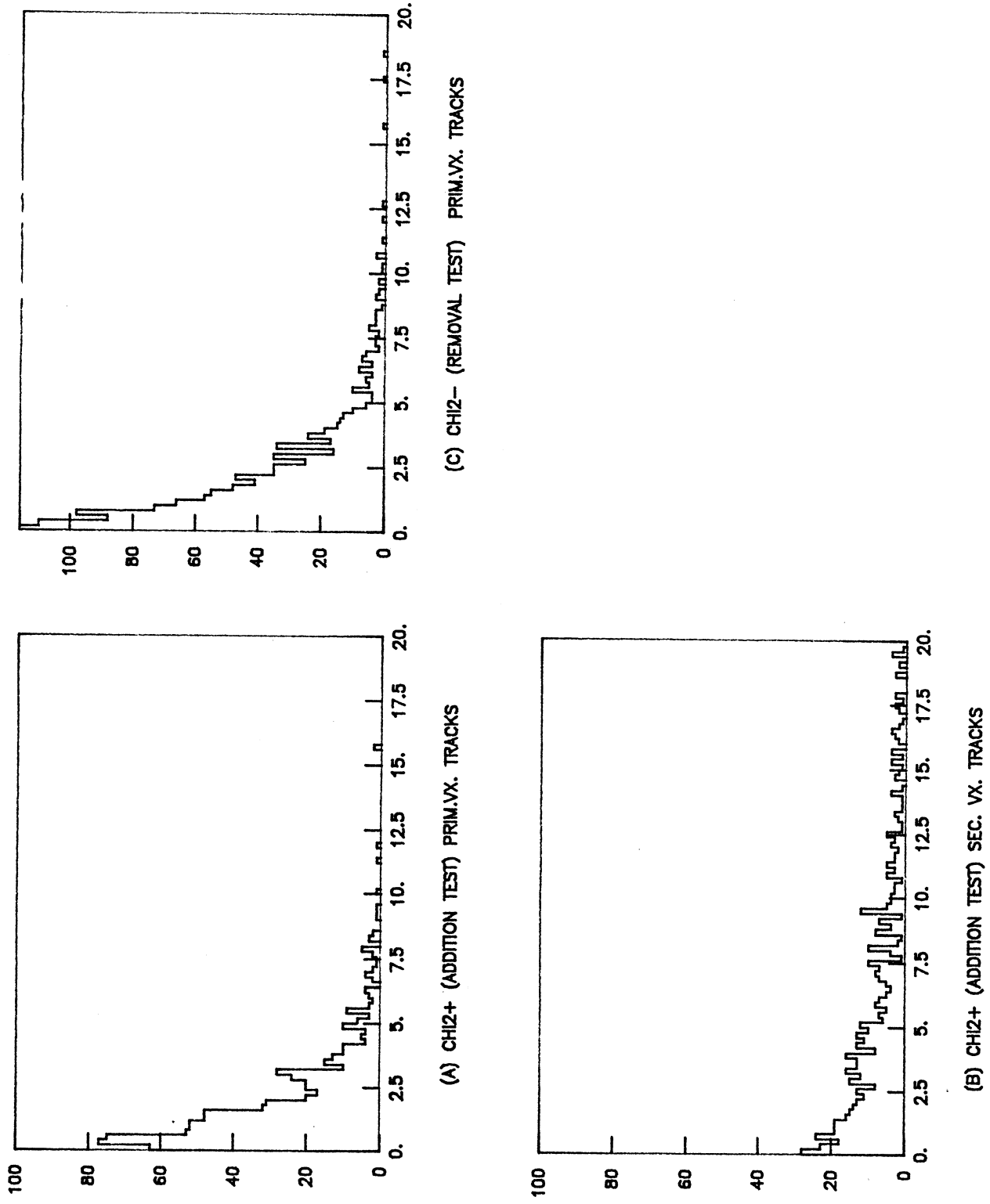


**Fig. 6** Testing track association to primary vertex: $|\chi^2_{\pm}|$ for data sample B

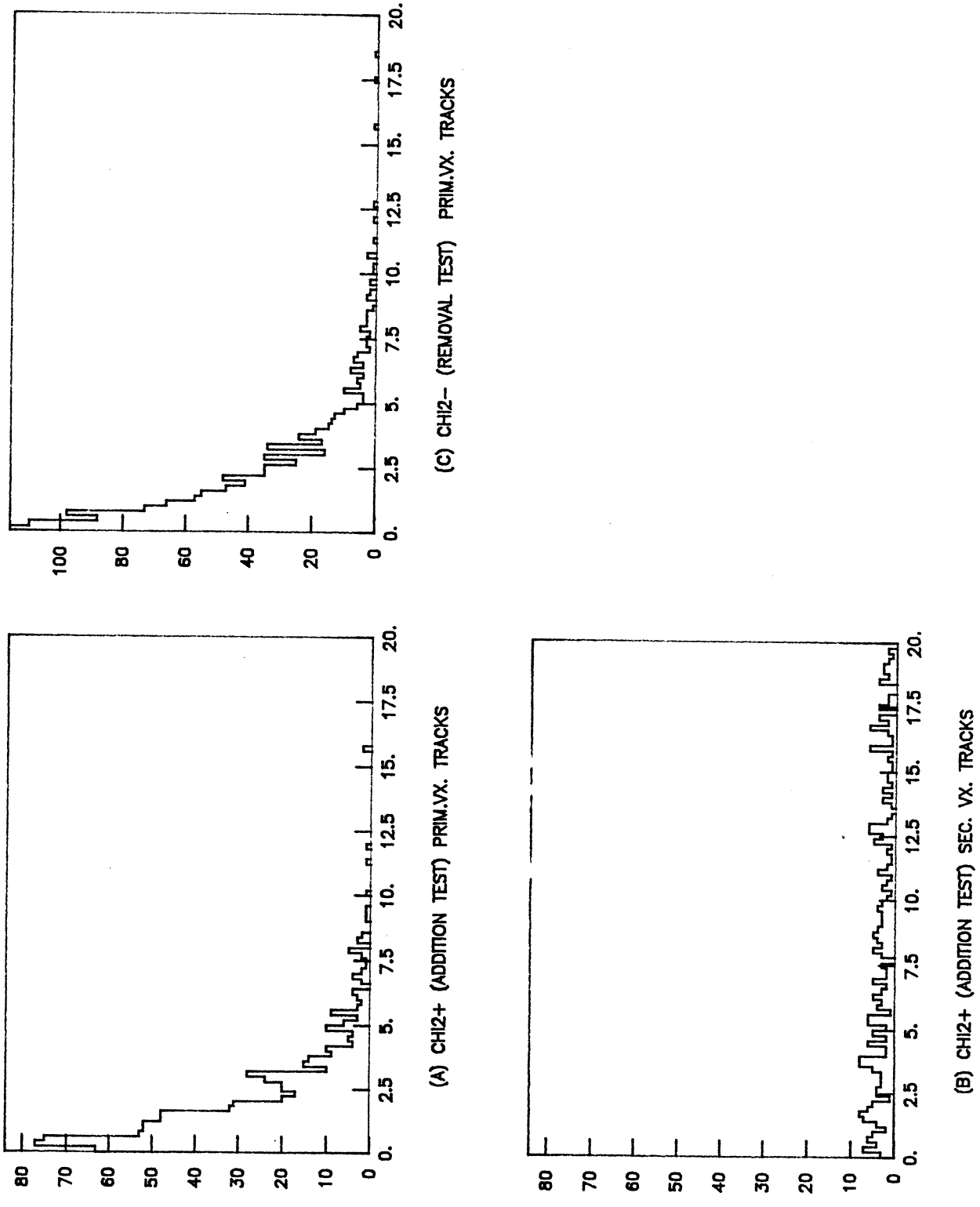


**Fig. 7** Testing track association to primary vertex: $|\chi^2_{\pm}|$ for data sample C

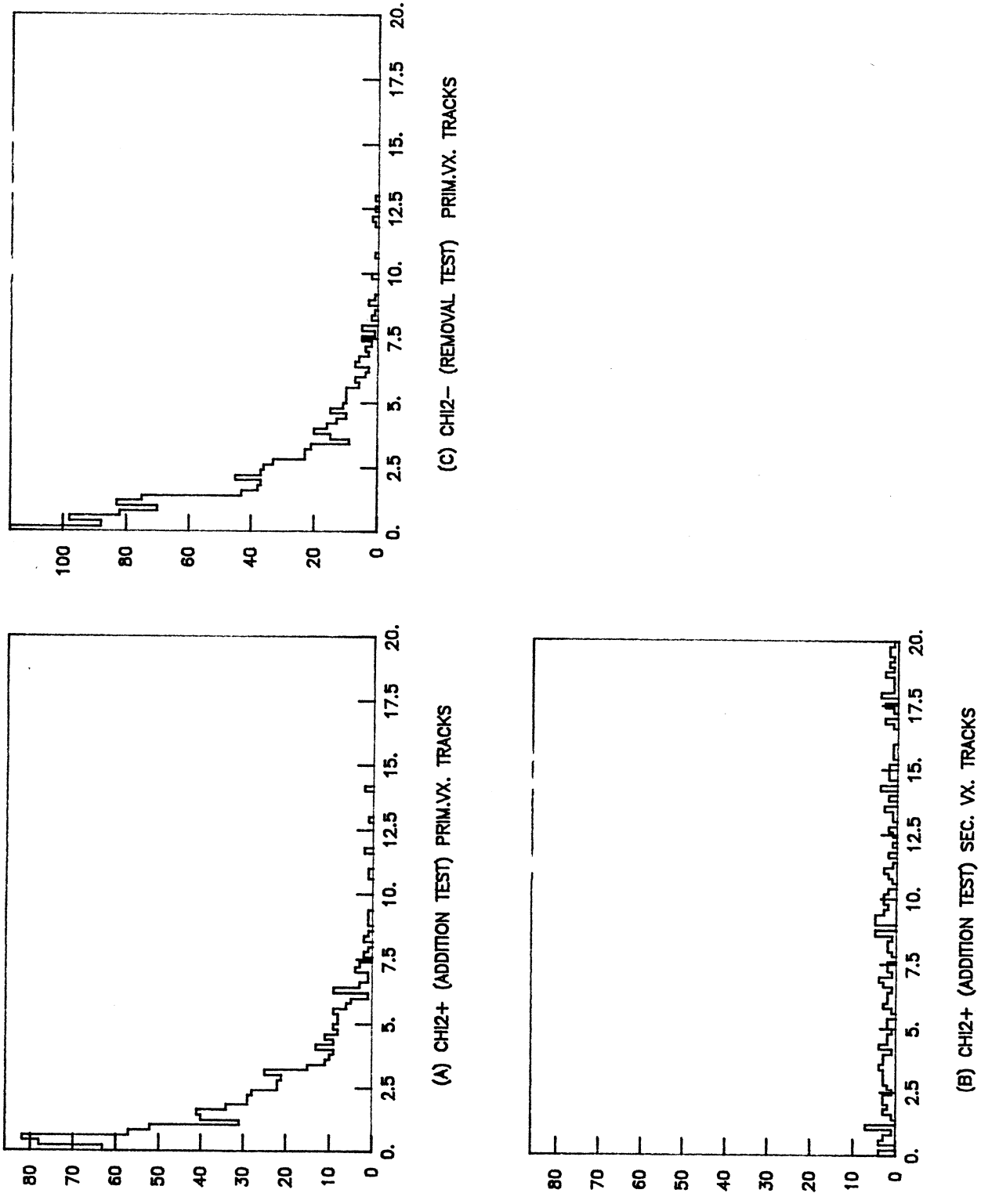


**Fig. 8** Testing track association to primary vertex: $|\chi^2_{\pm}|$ for data sample D

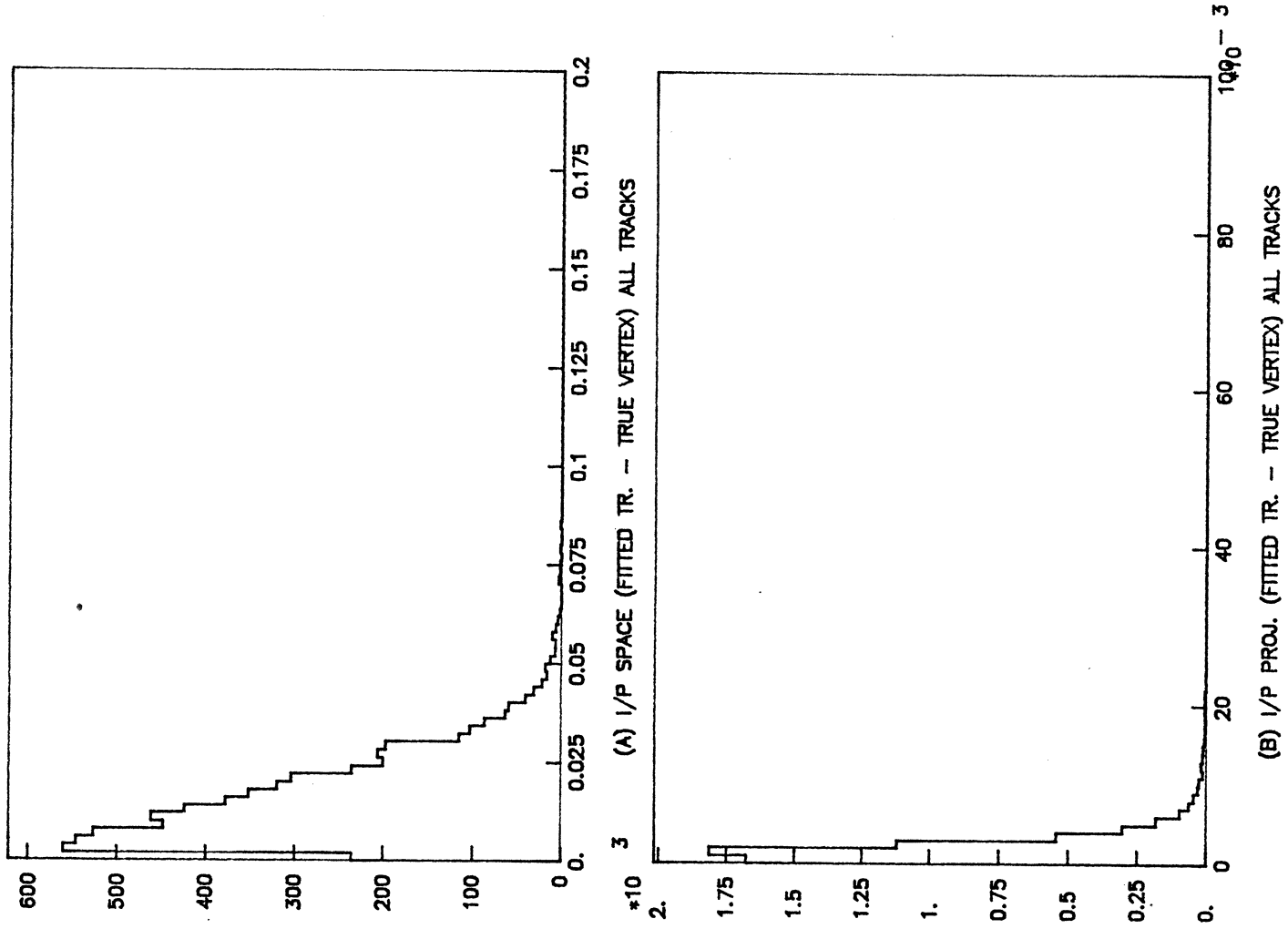


**Fig. 9** Impact parameters in space resp. projected, for data sample A

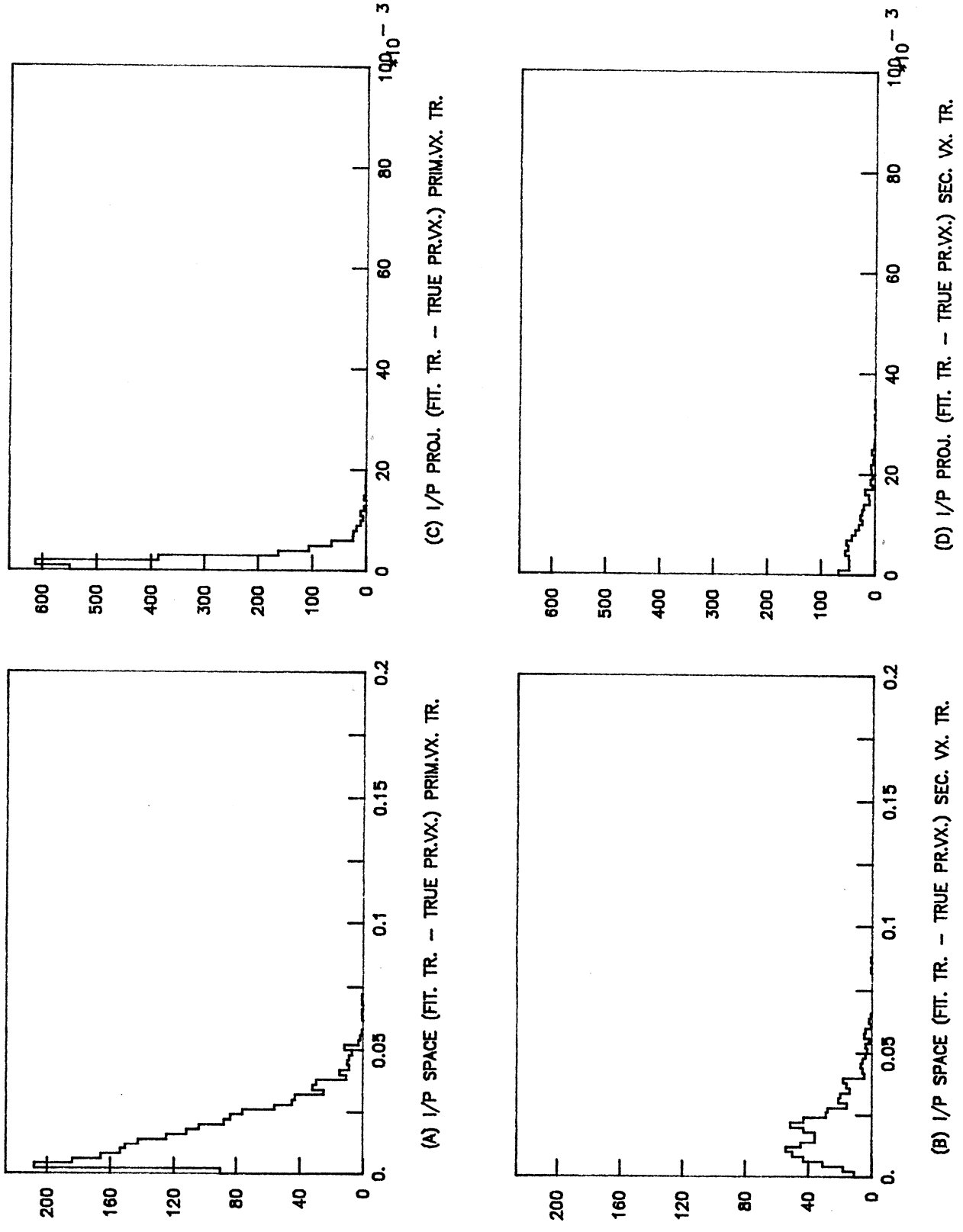


**Fig. 10** Impact parameters in space resp. projected, for data sample B

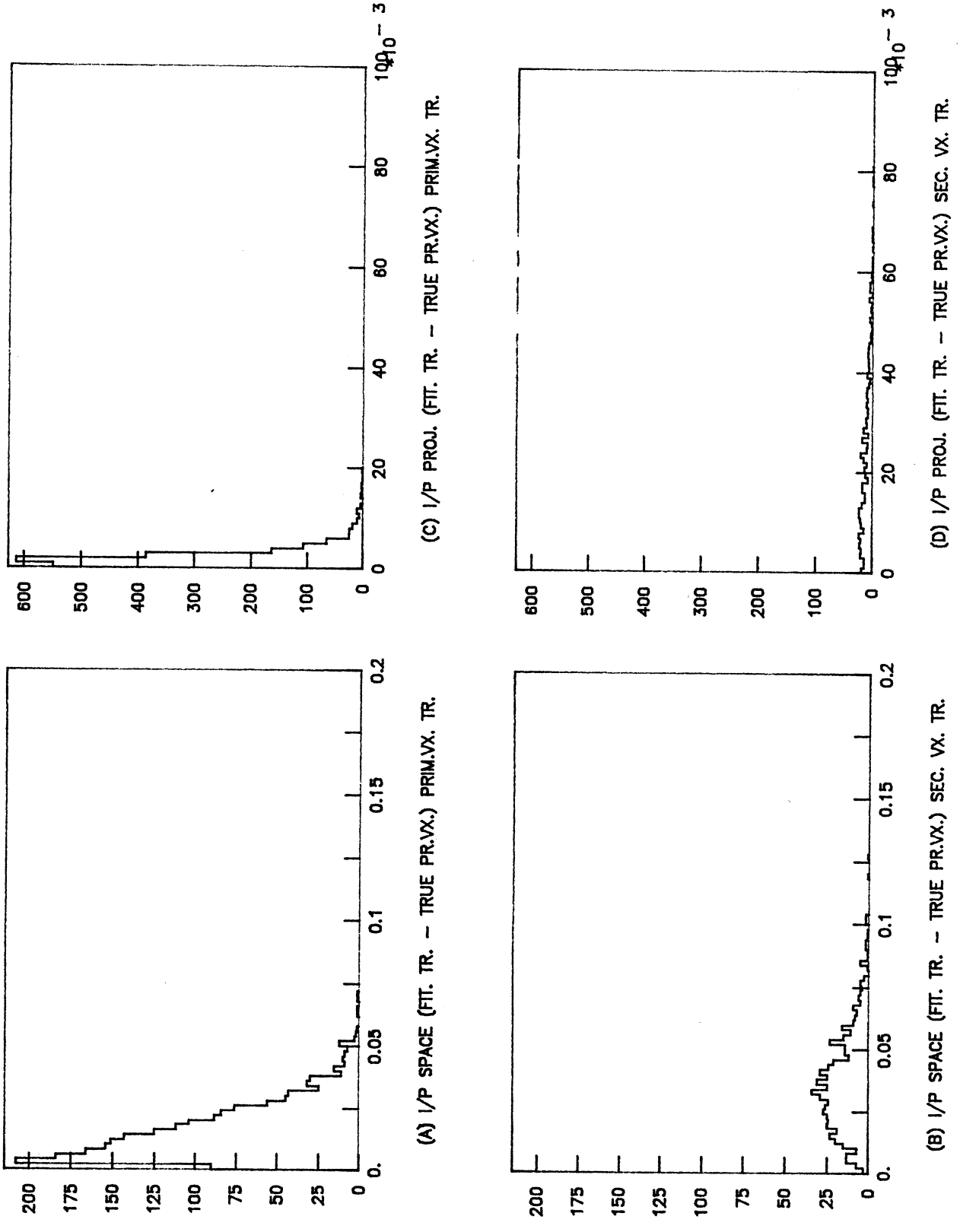


**Fig. 11** Impact parameters in space resp. projected, for data sample C

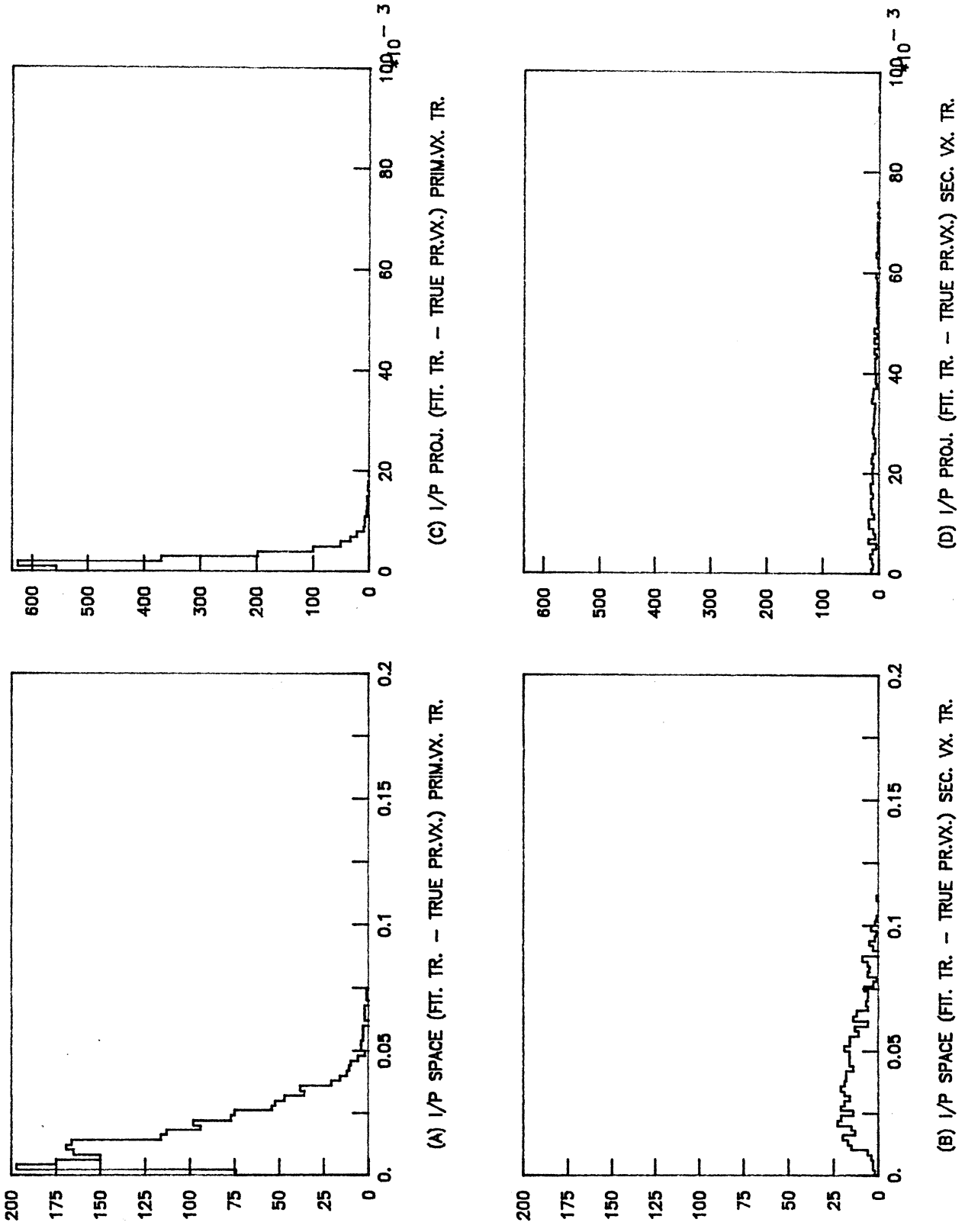


**Fig. 12** Impact parameters in space resp. projected, for data sample D